Widespread changes in Southern Ocean phytoplankton blooms linked to climate drivers

Sandy J. Thomalla [1,2] ✉, Sarah-Anne Nicholson [1], Thomas J. Ryan-Keogh [1] &
Marié E. Smith [3,4]

Climate change is expected to elicit widespread alterations to nutrient and light supply, which interact to influence phytoplankton growth and their seasonal cycles. Using 25 years of satellite chlorophyll *a* data, we show that large regions of the Southern Ocean express significant multi-decadal trends in phenological indices that are typically larger (<50 days decade^{-1}) than previously reported in modelling studies (<10 days decade^{-1}). Although regionally dependent, there is an overall tendency for phytoplankton blooms to increase in amplitude, decline in seasonality, initiate later, terminate earlier and have shorter durations, except in the ice, which initiate earlier and have longer durations. Investigating relationships with prominent climate drivers highlights regional sensitivities and complexities of multiple interacting aspects of a changing climate. Seasonal adjustments of this magnitude at the base of the food web can de-synchronize energy transfer to higher trophic levels, threatening ecosystem services and impacting global climate by altering natural CO_2 uptake.

Quantifying the strength and efficiency of the biological carbon pump (BCP) and its sensitivity to predicted changes in Earth's climate is fundamental to our ability to predict long-term changes in the global carbon cycle and, by extension, the impact of continued anthropogenic perturbation of atmospheric CO_2 levels[1,2]. The Southern Ocean plays a critical role in mitigating climate change impacts by taking up 50% of the oceanic uptake of CO_2 (refs. 3,4) and 75% of the excess heat generated by anthropogenic CO_2 (ref. 5). Southern Ocean phytoplankton primary production (PP) is important for sustaining biodiversity, fuelling the food web and driving natural carbon uptake. By exporting organic material into the ocean's interior, the BCP also regulates the supply of remineralized nutrients to surface waters, which in turn impacts lower-latitude PP and associated carbon export[6,7]. There is little agreement, however, in Earth system model projections of the climate sensitivity of the Southern Ocean BCP with a lack of consensus in the direction of predicted change in export flux[8], highlighting

gaps in our understanding and ability to accurately represent a major planetary carbon flux[9].

High rates of PP are a characteristic of the Southern Ocean, driven in part by high macronutrient availability and constrained by light and the micronutrient iron[10]. It is anticipated that anthropogenic forcing will increasingly influence oceanic nutrient cycling[11], impacting PP, ecosystem function and the transfer of carbon, energy and nutrients through the food web with complex feedbacks on ocean biogeochemistry and climate[12]. The Southern Ocean is considered to be particularly sensitive to climate change[13], with widespread physico-chemical changes already being observed in regional warming[14], increased vertical stratification and altered mixed-layer depths (MLDs) in response to stronger winds[15], iron limitation[16], freshening linked to changes in sea-ice extent[17], lowered pH[18] and altered cloud cover and irradiance[12]. The Southern Ocean is a vast and diverse environment with organisms being subject to multiple interacting aspects of these changes,

[1]Southern Ocean Carbon–Climate Observatory, CSIR, Cape Town, South Africa. [2]Marine and Antarctic Research Centre for Innovation and Sustainability, University of Cape Town, Cape Town, South Africa. [3]Coastal Systems and Earth Observation Research Group, CSIR, Cape Town, South Africa. [4]Department of Oceanography, University of Cape Town, Cape Town, South Africa. ✉e-mail: sandy.thomalla@gmail.com

the effects of which may be synergistic or antagonistic, making the net impact on phytoplankton diversity, abundance, productivity and export complex and difficult to determine[19].

The seasonal cycle sets much of the environmental variability in the factors that drive PP[20]. It is also the mode of variability that couples the physical mechanisms of climate forcing to ecosystem response in production, diversity and carbon export[21]. Accordingly, it is expected that any long-term trends in Southern Ocean productivity will be mediated through changes in the characteristics of the seasonal cycle and its interaction with the phenology of the ecosystem. Interrogating long-term alterations in the characteristics of the seasonal cycle is thus expected to provide a sensitive index of climate variability. The most widely used index of phenology is the start of the seasonal bloom, which can significantly impact the success of higher trophic levels that rely on plankton as their principal food source[22]. Other important metrics relate to the bloom amplitude and duration, which dictate the amount of biomass being generated within a season that can be exported to the ocean's interior or transferred to higher trophic levels via the marine food web[23]. Although modelling studies[24,25] have shown that 30–40 years of PP data are necessary to distinguish a climate change trend from background natural variability, others suggest that indicators such as phenology may detect trends more rapidly[24]. Indeed, a follow-up modelling study[26] found that from a global perspective, as little as 20 years of data were required to distinguish a trend in bloom initiation.

Remote sensing of ocean colour is currently the only observational capability that can provide synoptic views of upper-ocean phytoplankton at high spatial and temporal resolution and high temporal extent. In 2011, Thomalla et al.[27] used nine years of satellite chlorophyll a (chl-a) data (available at the time) to characterize the seasonal cycle of Southern Ocean phytoplankton in terms of bloom initiation, amplitude and variability. With an additional 16 years of data, we now have the means to not only characterize regional variability in seasonal indices, but also to investigate trends in those indices over the past 25 years. Understanding the spatial variability in multi-decadal trends in the characteristics of Southern Ocean blooms will provide a unique opportunity to assess regional differences in the response of the biogeochemical system to a changing climate.

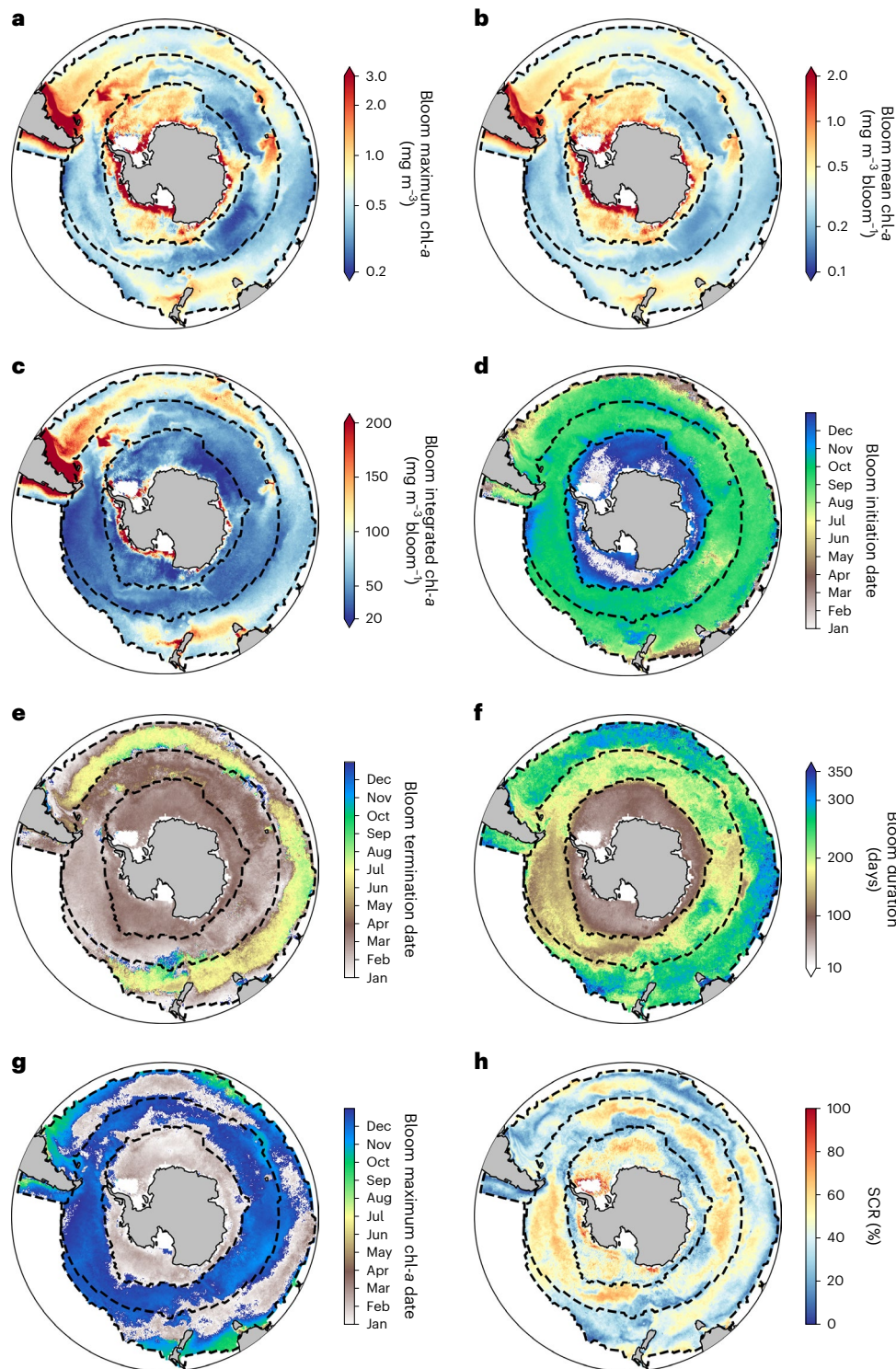## Trends in phytoplankton seasonal metrics

Using a range of criteria, Fay and McKinley[28] divided the Southern Ocean into three biomes: the subtropical seasonally stratified (STSS), the subpolar seasonally stratified (SPSS) and the ice (ICE). A large degree of spatial variability is evident in the mean distribution of seasonal metrics (bloom timing, amplitude and seasonality) derived from 25 years of chl-a data, which oftentimes differ between ocean basins (for example, shorter blooms of lower amplitude in the Pacific), zonally (for example, associated with the different biomes) and regionally (for example, at continental margins and subantarctic islands) (Fig. 1). This heterogeneity is considered to result primarily from distinct underlying physics that alters the light environment and dominant supply mechanisms of key nutrients, driving subsequent regional variability in phytoplankton growth and variegated bloom characteristics[27]. Determining how large-scale physical processes associated with climate adjustments manifest as ecological responses at smaller scales is critical for interpreting ecosystem variability and deciphering trends and trajectories in the BCP and trophodynamics. However, spatial and temporal irregularity in the characteristics of marine ecosystems makes detection of systematic changes in response to climate pressures challenging[29].

In this study, significant trends were detectable in all seasonal metrics, with spatial heterogeneity evident as regionally cohesive distributions of significantly positive or negative trends (Figs. 2 and 3 and Supplementary Table 1). This directional dominance in trend distribution is similarly evident in trends that are not significant ($P > 0.05$;

Extended Data Fig. 1) but that may become so when more years of data are available. Contrary to what has been suggested in modelling studies[24,26], significant trends in bloom magnitude (maximum, mean and integrated chl-a) were detectable from only 25 years of satellite data. Moreover, bloom magnitude metrics (maximum, mean and integrated chl-a) generally display a larger percentage significance than phenology metrics (initiation, termination, duration and peak timing). This disparity between model predictions and satellite observations may stem from the model's inability to accurately characterize the timing and amplitude of the Southern Ocean's seasonal cycle[30]. The predominance in positive trends in bloom magnitude (Figs. 2a–c and 3 and Extended Data Fig. 1) would arguably be associated with an increase in the amount of bulk carbon being produced during the seasonal bloom (for example, mean of positive significant trends in bloom integrated chl-a = +15 mg m^{-3} bloom^{-1} decade^{-1}, equating to an increase of 2.91% yr^{-1}; Supplementary Tables 1 and 2) and thus beneficial to both carbon export and fuelling the food web. However, an increase in chl-a is not necessarily associated with an increase in biomass, particularly in the iron and light co-limited Southern Ocean, where phytoplankton can adjust their cellular chl-a to carbon ratios in response to environmental stresses[16]. This ambiguity in translating trends in chl-a to trends in biomass is highlighted by the negative trends observed in net PP for much of the Southern Ocean (for the majority of satellite models)[16,31] and the negative trends in backscatter (b_{bp}) (as a proxy for carbon) for the STSS and SPSS biomes (Extended Data Fig. 2a), which accounts for the observed general increasing trend in chl-a/b_{bp} ratios (Extended Data Fig. 2b). Regardless, these trends in chl-a magnitude, whose positive distribution dominates in all biomes (Fig. 3 and Extended Data Fig. 1), reflect strong adjustments in phytoplankton in response to environmental conditions. Interestingly, the ICE biome has an increasing trend in b_{bp} (coincident with chl-a) in all but the Ross Sea, which is a highly productive and important region for the marine food web, with declining trends instead having the potential to negatively impact higher trophic levels.

Of note when interrogating the phenological trends is their magnitude (typically <50 days decade^{-1}; Fig. 2d–f), which is substantially larger than previous estimates from modelling studies (≤10 days decade^{-1}) (ref. 26). Indeed, only <6% of significant trends fell within a 10 day decade^{-1} range. Two example pixels (Extended Data Fig. 3a,b) provide a visual representation of a delayed bloom initiation and advances in maximum peak timing of 47 and 79 days decade^{-1}, respectively. The STSS and SPSS depict a predominance in the percentage significance of retreating bloom initiations (mean = −33 and −20 days decade^{-1}, respectively; Fig. 3 and Supplementary Table 1), which is contrary to what was predicted in two modelling studies that instead suggested a more regionally consistent trend (2006–2100) of advancing bloom initiations under IPCC representative concentration pathway 8.5 conditions[26,32]. These characteristics of retreating bloom initiations are coincident with a predominance in the percentage significant distribution of an advance in peak timing and termination, which drives a substantial contraction of bloom duration in the STSS and SPSS (mean = −53 and −20 days decade^{-1}, respectively; Figs. 2f and 3 and Supplementary Table 1). On the contrary, a predominance in the distribution of advancing bloom initiations in the ICE biome drives extended bloom durations (mean of significant positive trends in duration = +21 days decade^{-1}; Figs. 2d,f Fig. 3 and Supplementary Table 1). The sensitivity of these trends to the choice of method for detecting phenological metrics was investigated by comparing these trends with those derived from the cumulative-sum and rate-of-change methods[33]. Although in a mean sense some differences are evident in the regional distribution of seasonal metrics (Extended Data Fig. 4), when it comes to the trends, their distribution (Extended Data Fig. 5) and percentage significance (Extended Data Fig. 6) are similar across all methods.

Research emanating from the past decade has emphasized the important role that subseasonal temporal scales and meso- to
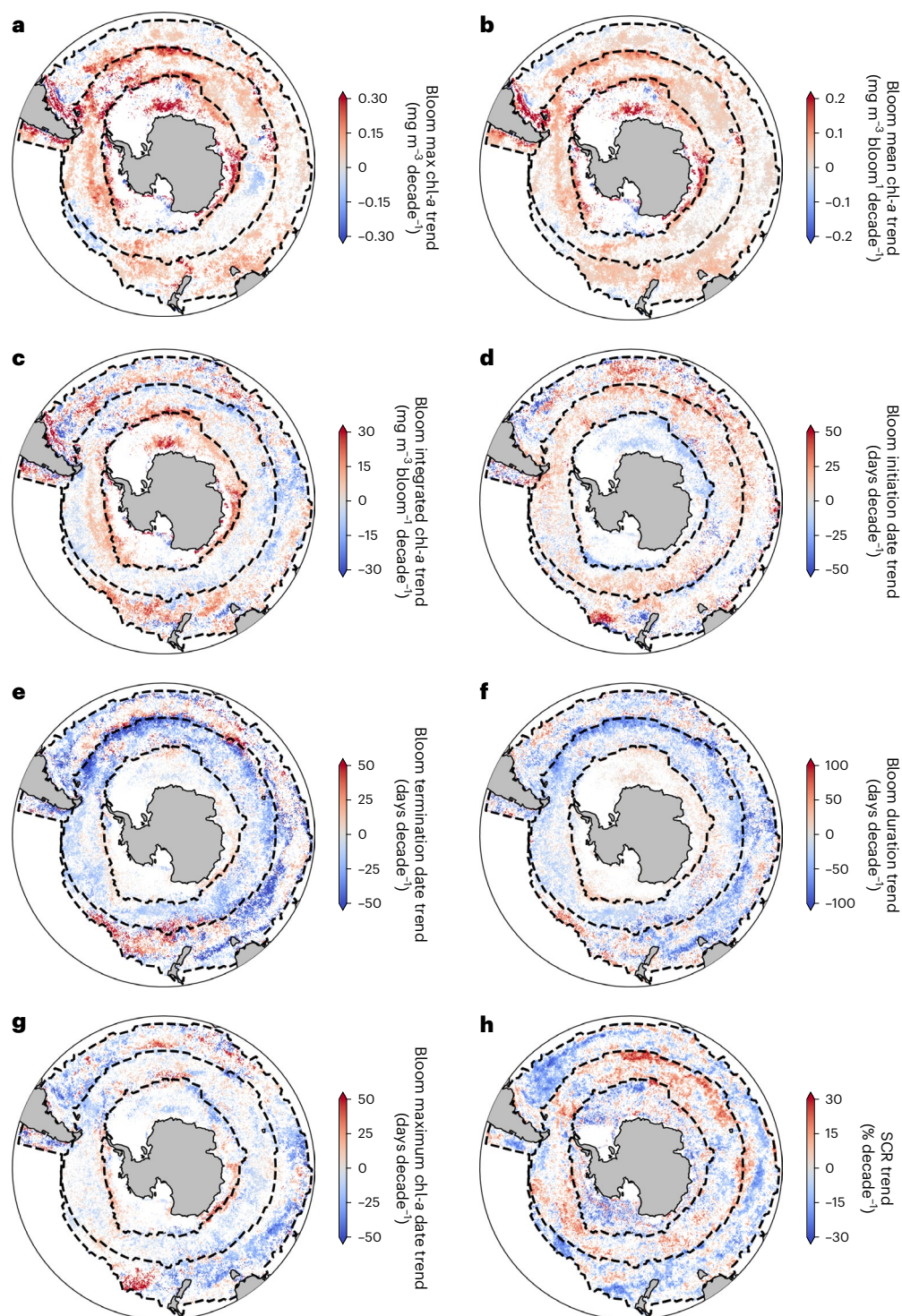
Fig. 1 | Regional distribution of phytoplankton seasonal metrics. a–h, Maps of mean (1998–2022) bloom max chl-*a* (**a**), mean chl-*a* over bloom duration (**b**), integrated chl-*a* over bloom duration (**c**), bloom initiation (**d**), bloom termination (**e**), bloom duration (**f**), bloom max chl-*a* date (**g**) and seasonal cycle reproducibility (SCR) (**h**). Phenological indices (**b–f**) are determined using the threshold method of detection; for other methods, see Extended Data Fig. 4. Dashed lines depict the boundaries of the Fay and McKinley[28] Southern Ocean biomes from north to south as the STSS, the SPSS and the ICE.

submeso-spatial scales play in characterizing the seasonal cycle of upper-ocean physics and biogeochemical response in the Southern Ocean[34–44]. The degree of seasonal cycle reproducibility (SCR) (calculated as the correlation between the observed annual time series and the mean climatological seasonal cycle)[27] is a useful metric that can capture these important scales of variability and reflect the characteristics

of dominant seasonal versus subseasonal supply mechanisms[27]. An example pixel (Extended Data Fig. 3c) provides a visual representation of a decline in SCR of 29% decade^{-1}. Trends in SCR in the STSS and ICE biomes (Figs. 2h and 3, Extended Data Fig. 1 and Supplementary Table 1) suggest a predominance in declining SCR (mean of significant negative trends = −12% decade^{-1} and −20% decade^{-1}, respectively),

Fig. 2 | Regional distribution of trends in phytoplankton seasonal metrics. **a**–**h**, Decadal trends (1998–2022) of bloom max chl-*a* (**a**), mean chl-*a* over bloom duration (**b**), integrated chl-*a* over bloom duration (**c**), bloom initiation (**d**), bloom termination (**e**), bloom duration (**f**), bloom max chl-*a* date (**g**) and seasonal cycle reproducibility (SCR) (**h**). Phenological indices (**b**–**f**) are determined using the threshold method of detection; for other methods, see Extended Data Figs. 5 and 6. Dashed lines depict the boundaries of the Fay and McKinley[28] Southern Ocean biomes from north to south as the STSS, the SPSS and the ICE. Only pixels where trends were significant ($P < 0.05$) and where >50% of the time series per year was available have been plotted; non-significant trends ($P > 0.05$) and incomplete time series are presented as white.

which implies a shift in the characteristics of the seasonal cycle to one that is more variable and less predictable. On the contrary, the SPSS biome suggests a predominance in trends of increasing SCR (mean of significant positive trends = +14% decade⁻¹) and adjustments towards a less variable seasonal cycle. Two modified approaches to calculating

SCR (as the correlation against a detrended and 5 yr rolling climatology) tested the robustness of the trends and susceptibility of the method to possible bias. Although some discrepancies exist in the climatological distribution of mean SCR (Extended Data Fig. 7b), there is little difference in the proportional distribution of observed trends, which retain
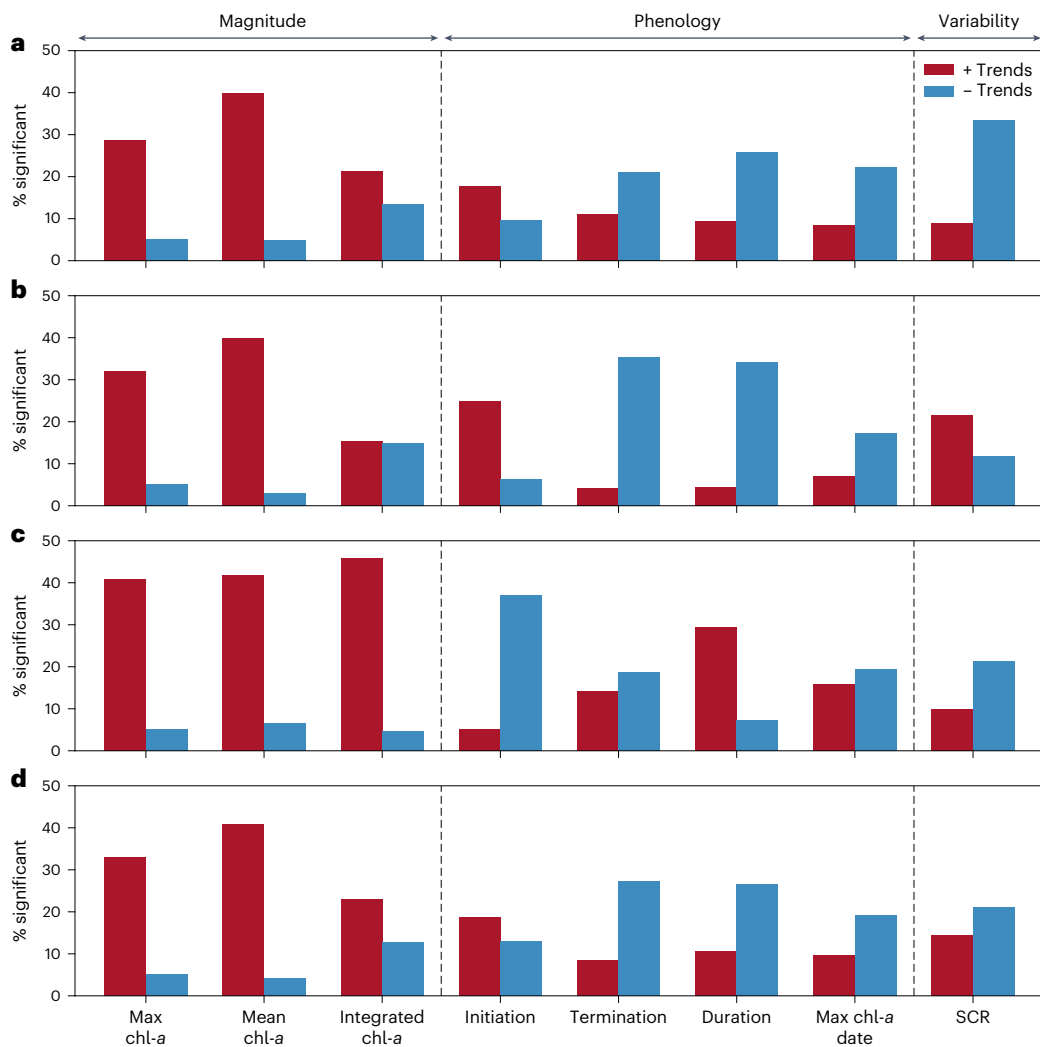
Fig. 3 | Bar graph highlighting regional dominance in the direction of significant trends in phytoplankton seasonal metrics. a–d, Bars depict the percentage of pixels with significant ($P < 0.05$) positive (red) or negative (blue) trends per seasonal metric relative to the total number of pixels per biome and for the Southern Ocean as a whole for the Fay and McKinley[28] biomes STSS (**a**), SPSS (**b**), ICE (**c**) and all three biomes merged (**d**). Phenological indices are determined using the threshold method of detection; for other methods, please see Extended Data Figs. 6. The % significant values are available in Supplementary Table 1 together with the mean significant trend per metric for each biome and for the Southern Ocean as a whole.

a relative predominance in declining SCR (Extended Data Figs. 7d and 8). These results suggest that the seasonal characteristics of vast areas of the Southern Ocean are evolving to reflect changes in the degree of environmental variability that may lead to alterations in biomass and phytoplankton diversity (for example, from competitive exclusion[45]). Climate-induced shifts in phytoplankton species composition are key as cell size and elemental stoichiometry impose fundamental constraints on growth rates, food web structure and trophic-level interactions that determine the trajectory of carbon through the food web and the proportion of biomass being exported[46]. An example is the observed decline in mean size and a reduction of diatoms in the western Antarctic[47] associated with a thinning and retreat of the ice sheet over the past decade[48]. These changes are particularly important in the Southern Ocean, where many of the world's water masses are formed and the biogeochemical cycling of organic material dictates surface water nutrient supply[7].

Linking climate drivers to trends in seasonal metrics

Of the most prominent climate-driven adjustments to Southern Ocean conditions are a general warming[49], an intensification and southward shift of the westerly winds in association with a more positive phase of the Southern Annular Mode[50] and an increase in stratification and deepening of the summer MLD[15]. All phenological trends reflect the integrated impact of a suite of concurrent physical, chemical and biological processes that may be nonlinear, synergistic or antagonistic and may reflect correlation rather than causation. This makes it challenging to attribute observed trends in the characteristics of the seasonal cycle to a specific mechanistic driver. Nevertheless, with these dominant drivers in mind (Extended Data Fig. 9), we investigate their relationship with bloom duration (which represents both initiation and termination), mean bloom chl-a (the largest percentage significance of the chl-a metrics) and SCR (Fig. 4) (all other correlation maps are available in Extended Data Fig. 10).

Results highlight the regional heterogeneity of driver relationships that do not typically hold across biomes. Trends in mean bloom chl-a were correlated with sea surface temperature (SST) for large regions of the Southern Ocean (Fig. 4a) (similarly noted by ref. 31), which may reflect enhanced metabolic activity in response to warming[51]. The correlations of mean bloom chl-a with summer MLDs (Fig. 4b) and windiness (Fig. 4c) were patchy, with the variegated response in the sign of the correlation probably reflecting regional dependence in the degree
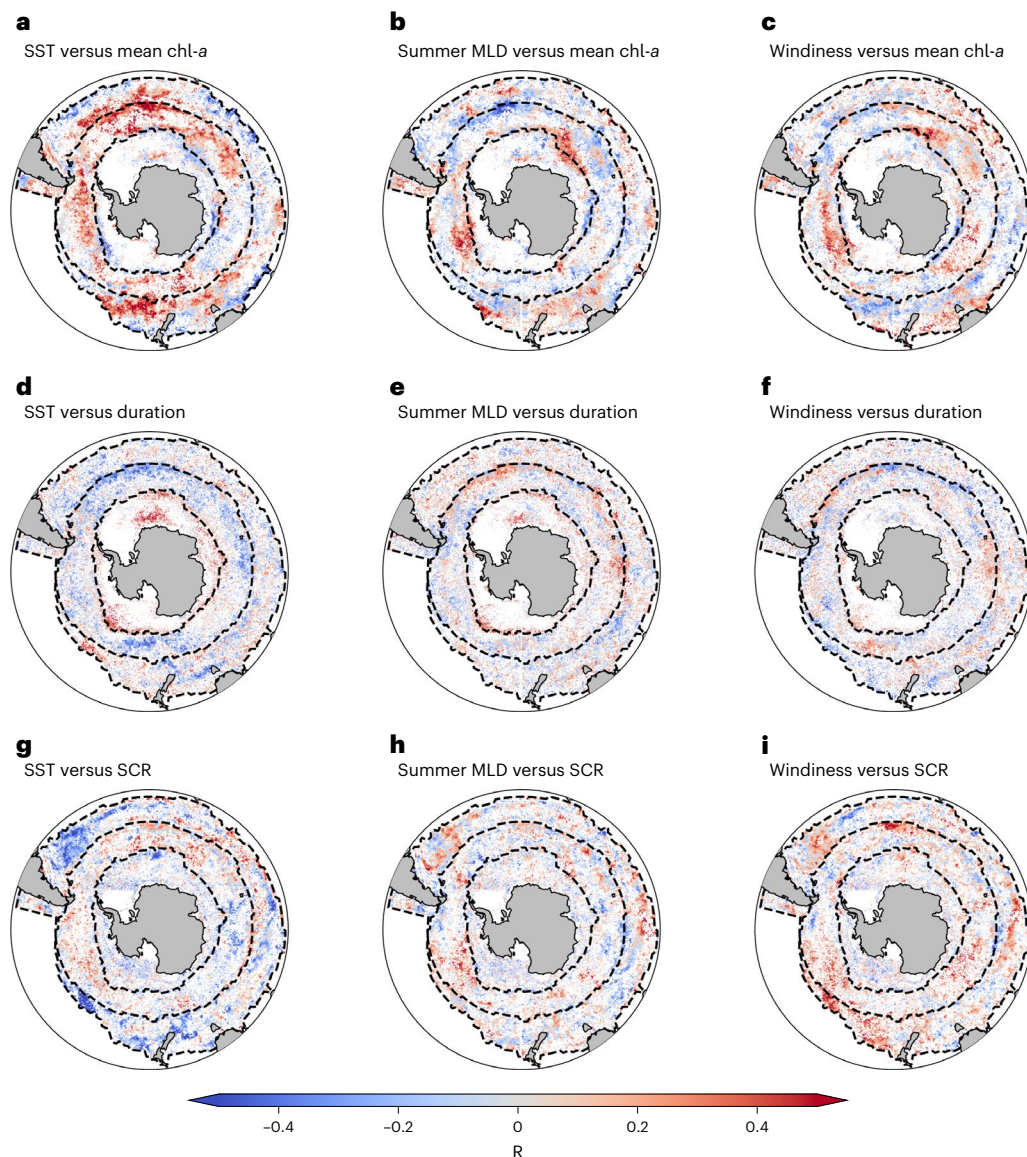
Fig. 4 | Regional distribution of correlation between physical drivers and a subset of phytoplankton seasonal metrics. a–i, Maps depict the spatial correlation of mean bloom chlorophyll (chl-*a*) (**a**,**b**,**c**), bloom duration (**d**,**e**,**f**) and SCR (**g**,**h**,**i**) against SST (**a**,**d**,**g**), summer MLD (**b**,**e**,**h**) and windiness (the number of days per year that wind was greater than the 25 yr 75th percentile) (**c**,**f**,**i**). Data were excluded if less than 50% of either time series per year was available. Correlations are performed against the corresponding 25 years of SST, MLD and windiness data (1998–2022), with data plotted only if the seasonal cycle metric trend is significant. For other phenological metrics, please see Extended Data Fig. 10.

of nutrient versus light limitation (for example, ref. 52). Correlations with bloom duration were typically weak, with a generally consistent positive relationship observed with SST and summer MLD in the ICE biome (Fig. 4d,e), which is anticipated to be linked to trends in sea-ice concentration and extent[53], the onset of ice melt[54] and advancing bloom initiations (Fig. 3c). Negative correlations between SST and trends in SCR typically align with positive correlations in windiness (Fig. 4g,i). There is some evidence of regional coherence in the trends of windiness and deeper summer MLDs, most notably upstream of the Drake Passage and the Weddell gyre (Extended Data Fig. 9), with a concomitant decline in SCR (Figs. 2h and 4h,i) that may reflect the reported increase in the number and intensity of low-level cyclones around the South Shetland Islands over the past 30 years[27,55].

Decadal changes to seasonal regimes

More than a decade ago, Thomalla et al.[27] concluded their study with a synthesis schematic that divided the Southern Ocean into a montage of

four regions that summarized the varying responses of phytoplankton biomass to different seasonal regimes. We are now able to reproduce that same schematic to explore decadal changes (Fig. 5), with the most notable differences being a decrease in regions of low chl-*a* and an increase in the spatial extent of regions characterized by high chl-*a* and low SCR (Fig. 5d,e). There are substantial differences in the spatial distribution of these adjustments, with a strong zonal coherence (Fig. 5c,e) that may reflect the poleward displacement of fronts within the Antarctic Circumpolar Current over the past 20 years[56]. These results suggest an increase in the role of subseasonal temporal scales and meso- to submeso-spatial scales, which is in agreement with a significant increase in Southern Ocean eddy activity attributed to a strengthening of the wind stress since the early 1990s[49]. Physical modifications such as these are likely to alter the intra-seasonal characteristics of light and nutrient supply, thereby impacting phytoplankton growth. This deduction is supported by growing evidence suggesting that in addition to deep winter mixing[57], storm-driven entrainment
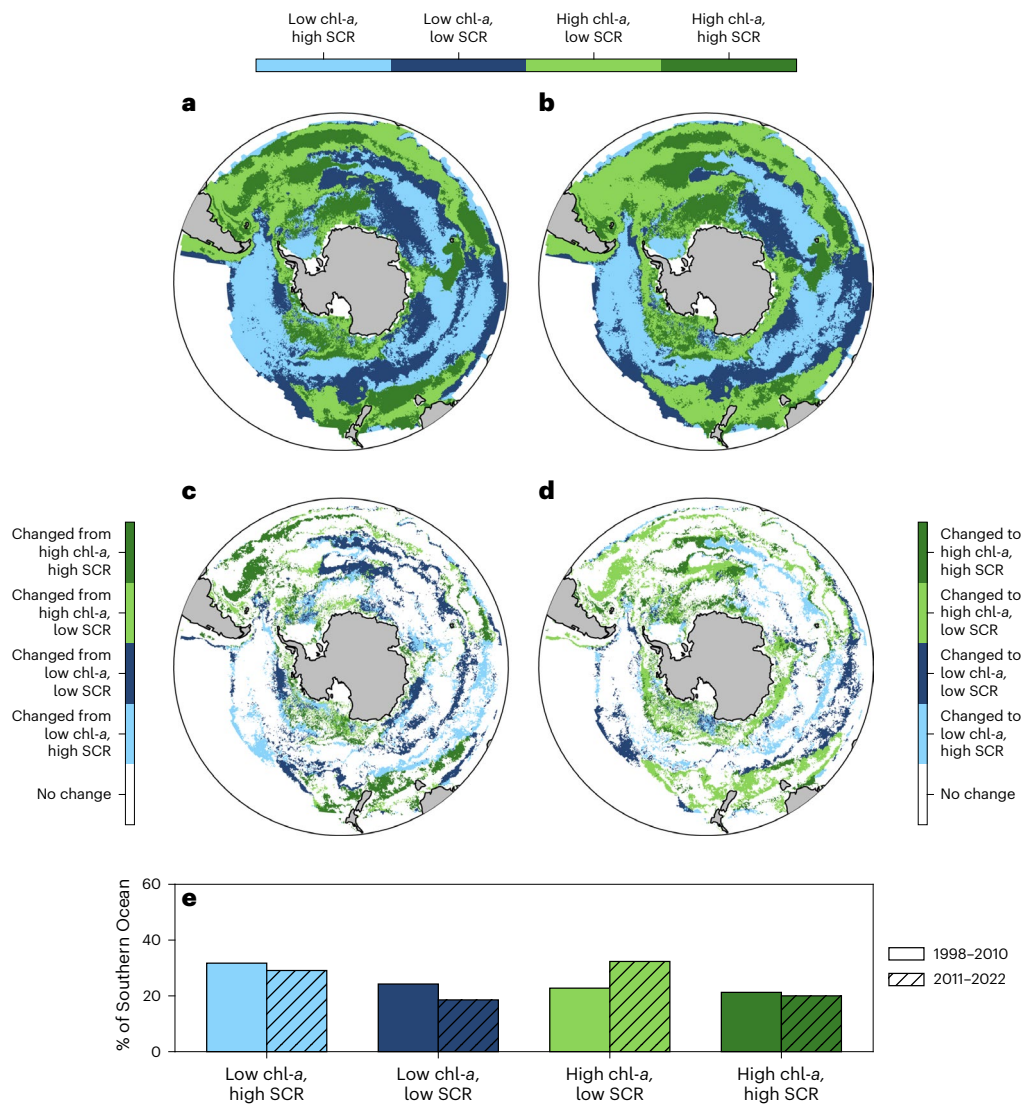
Fig. 5 | A schematic that summarizes the response of phytoplankton biomass to different seasonal regimes (classified according to their characteristics of variability) and how this regional classification has changed over 25 years. a,b, The regional classifications for 1998–2010 (**a**) and 2011–2022 (**b**). Regions in blue represent regions of low (<0.25 mg m^{-3}) chl-*a* concentration with either high SCR (>40%) (Region A, light blue) or low SCR (<40%) (Region B, dark blue). Regions in green represent regions of high chl-*a* concentration (>0.25 mg m^{-3}) with either low SCR (Region C, light green) or high SCR (Region D, dark green). **c,d**, The two schematics highlight the regions that changed their classification between 1998–2010 and 2011–2022 and indicate what they changed from **c** and what they changed to **d**. **e**, A bar chart showing the percentage of the Southern Ocean that was classified as each of the four regions between the different periods.

Ecological impacts of widespread trends in seasonal metrics

These trends in the characteristics of the Southern Ocean seasonal cycle reflect changes in environmental conditions that alter the drivers of phytoplankton production, abundance and community composition, with feedbacks that threaten the ecosystem services they provide: sustaining biodiversity, fuelling the food web and mediating global climate through an altered efficiency of the BCP[19]. Support of higher trophic levels is of particular relevance in this region as phytoplankton PP sustains a rich and diverse food web dominated by krill, marine birds, seals and migratory whales. As top predators, Weddell seals integrate information across the entire trophic web with the isotopic composition of their diet being preserved in the archive of their pelts[60]. A stable isotope analysis by Huckstadt et al.[61] found a significant decline in the

isotopic characteristics of the diet of Weddell seals in the Ross Sea over the past 100 years, which was linked to widespread changes in upwelled nutrient supply, PP and phytoplankton community structure. These findings emphasize the cascading impact of climate adjustments in environmental conditions through the food web from the trophic base to top predators.

The predominance of shorter blooms for the Southern Ocean as a whole (Fig. 3) is expected to have negative implications for carbon drawdown and trophic supply. Indeed, the duration of the seasonal bloom is proposed to be more important for carbon storage and sequestration than the magnitude[47] as longer mealtimes for consumers lead to larger proportions of the bloom being stored in animals as opposed to being reworked through the microbial loop[23]. These phenological trends also have the potential to negatively impact the survival rate of zooplankton and larval fish populations if prey availability decouples from critical life stages[62–64]. Such impacts are transferred through trophic webs with important implications for a number of key

species whose timing of spring migrations and breeding phenologies relies heavily on the quantity and quality of marine food sources. For example, seabirds in east Antarctica are delaying their arrival at their colonies by 1.6 days decade^{-1} and their first egg laying by 0.4 days decade^{-1}. These delays are linked to a regional decrease in sea-ice extent and an increase in sea-ice duration, which together reduce the quantity and accessibility of food supplies in early spring[65]. Similarly, humpback whales integrate a multitude of environmental signals into their migratory decisions[66,67] with evidence of a one-month advance (1.5 days earlier per year) in departure from their Antarctic peninsula feeding grounds being linked to a reduction in krill abundance in response to the decreasing mass of the autumn ice sheet[68].

The consequences of changes to the timing, quantity and quality of their food source feed back into these higher trophic levels impacting their nutritional stress, reproductive success and survival rates; particularly if they are unable to synchronize their feeding and breeding patterns with that of their food supplies[65,69,70]. In addition to gradual changes engendered by global warming, climate forcing may produce rapid shifts in oceanographic and food-chain dynamics, driving alternative trophic pathways[70]. The absence of any definitive answers from the driver analysis highlights the complexities of multiple interacting aspects of a changing climate. Nonetheless, the trends in seasonal metrics observed here are anticipated to continue or accelerate as climate change drives further adjustments in Southern Ocean physico-chemical conditions. These investigations provide a unique assessment of the response of seasonal bloom characteristics to climate drivers highlighting regional sensitivities that demand our attention in the context of the ecological impacts that such changes are expected to elicit on the BCP and trophic interactions.

Online content

Any methods, additional references, Nature Portfolio reporting summaries, source data, extended data, supplementary information, acknowledgements, peer review information; details of author contributions and competing interests; and statements of data and code availability are available at https://doi.org/10.1038/s41558-023-01768-4.

References

1. Henson, S. A. et al. A reduced estimate of the strength of the ocean's biological carbon pump. *Geophys. Res. Lett.* **38**, L04606 (2011).
2. Laufkötter, C., John, J. G., Stock, C. A. & Dunne, J. P. Temperature and oxygen dependence of the remineralization of organic matter. *Global Biogeochem. Cy.* **31**, 1038–1050 (2017).
3. Gruber, N., Landschützer, P. & Lovenduski, N. S. The variable Southern Ocean carbon sink. *Ann. Rev. Mar. Sci.* **11**, 159–186 (2019).
4. Gregor, L., Lebehot, A. D., Kok, S. & Scheel Monteiro, P. M. A comparative assessment of the uncertainties of global surface ocean CO$_2$ estimates using a machine-learning ensemble (CSIR-ML6 version 2019a)—have we hit the wall? *Geosci. Model Dev.* **12**, 5113–5136 (2019).
5. Frölicher, T. L. et al. Dominance of the Southern Ocean in anthropogenic carbon and heat uptake in CMIP5 models. *J. Clim.* **28**, 862–886 (2015).
6. Sarmiento, J. L., Gruber, N., Brzezinski, M. A. & Dunne, J. P. High-latitude controls of thermocline nutrients and low latitude biological productivity. *Nature* **427**, 56–60 (2004).
7. Leung, S. W., Weber, T., Cram, J. A. & Deutsch, C. Variable particle size distributions reduce the sensitivity of global export flux to climate change. *Biogeosciences* **18**, 229–250 (2021).
8. Henson, S. A. et al. Uncertain response of ocean biological carbon export in a changing world. *Nat. Geosci.* **15**, 248–254 (2022).
9. IPCC *Climate Change 2021: The Physical Science Basis* (eds Masson-Delmotte, V. et al.) (Cambridge Univ. Press, 2021).
10. Boyd, P. W. Environmental factors controlling phytoplankton processes in the Southern Ocean. *J. Phycol.* **38**, 844–861 (2002).
11. Krishnamurthy, A. et al. Impacts of increasing anthropogenic soluble iron and nitrogen deposition on ocean biogeochemistry. *Global Biogeochem. Cy.* **23**, GB3016 (2009).
12. Henley, S. F. et al. Changing biogeochemistry of the Southern Ocean and its ecosystem implications. *Front. Mar. Sci.* **7**, 581 (2020).
13. Marinov, I., Gnanadesikan, A., Toggweiler, J. R. & Sarmiento, J. L. The Southern Ocean biogeochemical divide. *Nature* **441**, 964–967 (2006).
14. Auger, M., Morrow, R., Kestenare, E., Sallée, J.-B. & Cowley, R. Southern Ocean in-situ temperature trends over 25 years emerge from interannual variability. *Nat. Commun.* **12**, 514 (2021).
15. Sallée, J.-B. et al. Summertime increases in upper-ocean stratification and mixed-layer depth. *Nature* **591**, 592–598 (2021).
16. Ryan-Keogh, T. J., Thomalla, S. J., Monteiro, P. M. S. & Tagliabue, A. Multidecadal trend of increasing iron stress in Southern Ocean phytoplankton. *Science* **379**, 834–840 (2023).
17. Haumann, F. A., Gruber, N. & Münnich, M. Sea-ice induced Southern Ocean subsurface warming and surface cooling in a warming climate. *AGU Adv.* **1**, e2019AV000132 (2020).
18. Bindoff, N. L. et al. in *Special Report on the Ocean and Cryosphere in a Changing Climate* (eds Pörtner, H.-O. et al.) 477–587 (IPCC, 2019).
19. Moline, M. A., Claustre, H., Frazer, T. K., Schofield, O. & Vernet, M. Alteration of the food web along the Antarctic Peninsula in response to a regional warming trend. *Glob. Change Biol.* **10**, 1973–1980 (2004).
20. Rodgers, K. B. et al. A wintertime uptake window for anthropogenic CO$_2$ in the North Pacific. *Global Biogeochem. Cy.* **22**, GB2020 (2008).
21. Monteiro, P. M. S., Boyd, P. & Bellerby, R. Role of the seasonal cycle in coupling climate and carbon cycling in the subantarctic zone. *Eos* **92**, 235–236 (2011).
22. Cushing, D. H. in *Advances in Marine Biology* Vol. 26 (eds Blaxter, J. H. S. & Southward, A. J.) 249–293 (Academic Press, 1990).
23. Barnes, D. K. A. in *Carbon Capture, Utilization and Sequestration* (ed. Agarwal, R. K.) Ch. 3 (IntechOpen, 2018); https://doi.org/10.5772/intechopen.78237
24. Henson, S. A. et al. Detection of anthropogenic climate change in satellite records of ocean chlorophyll and productivity. *Biogeosciences* **7**, 621–640 (2010).
25. Del Castillo, C. E., Signorini, S. R., Karaköylü, E. M. & Rivero-Calle, S. Is the Southern Ocean getting greener? *Geophys. Res. Lett.* **46**, 6034–6040 (2019).
26. Henson, S. A., Cole, H. S., Hopkins, J., Martin, A. P. & Yool, A. Detection of climate change-driven trends in phytoplankton phenology. *Glob. Change Biol.* **24**, e101–e111 (2018).
27. Thomalla, S. J., Fauchereau, N., Swart, S. & Monteiro, P. M. S. Regional scale characteristics of the seasonal cycle of chlorophyll in the Southern Ocean. *Biogeosciences* **8**, 2849–2866 (2011).
28. Fay, A. R. & McKinley, G. A. Global open-ocean biomes: mean and temporal variability. *Earth Syst. Sci. Data* **6**, 273–284 (2014).
29. Reid, K. & Croxall, J. P. Environmental response of upper trophic-level predators reveals a system change in an Antarctic marine ecosystem. *Proc. R. Soc. Lond. B* **268**, 377–384 (2001).
30. Hague, M. & Vichi, M. A link between CMIP5 phytoplankton phenology and sea ice in the Atlantic Southern Ocean. *Geophys. Res. Lett.* **45**, 6566–6575 (2018).
31. Pinkerton, M. H. et al. Evidence for the impact of climate change on primary producers in the Southern Ocean. *Front. Ecol. Evol.* **9**, 592027 (2021).
32. Yamaguchi, R. et al. Trophic level decoupling drives future changes in phytoplankton bloom phenology. *Nat. Clim. Change* **12**, 469–476 (2022).

33. Brody, S. R., Lozier, M. S. & Dunne, J. P. A comparison of methods to determine phytoplankton bloom initiation. *J. Geophys. Res. Oceans* **118**, 2345–2357 (2013).

34. Whitt, D. B., Nicholson, S. A. & Carranza, M. M. Global impacts of subseasonal (<60 day) wind variability on ocean surface stress, buoyancy flux, and mixed layer depth. *J. Geophys. Res. Oceans* **124**, 8798–8831 (2019).

35. Nicholson, S.-A., Lévy, M., Llort, J., Swart, S. & Monteiro, P. M. S. Investigation into the impact of storms on sustaining summer primary productivity in the sub-Antarctic Ocean. *Geophys. Res. Lett.* **43**, 9192–9199 (2016).

36. Nicholson, S.-A. et al. Iron supply pathways between the surface and subsurface waters of the Southern Ocean: from winter entrainment to summer storms. *Geophys. Res. Lett.* **46**, 14567–14575 (2019).

37. Swart, S., Thomalla, S. J. & Monteiro, P. M. S. The seasonal cycle of mixed layer dynamics and phytoplankton biomass in the sub-Antarctic zone: a high-resolution glider experiment. *J. Mar. Syst.* **147**, 103–115 (2015).

38. Thomalla, S. J., Racault, M., Swart, S. & Monteiro, P. M. S. High-resolution view of the spring bloom initiation and net community production in the subantarctic Southern Ocean using glider data. *ICES J. Mar. Sci.* **72**, 1999–2020 (2015).

39. du Plessis, M., Swart, S., Ansorge, I. J. & Mahadevan, A. Submesoscale processes promote seasonal restratification in the subantarctic Ocean. *J. Geophys. Res. Oceans* **122**, 2960–2975 (2017).

40. du Plessis, M., Swart, S., Ansorge, I. J., Mahadevan, A. & Thompson, A. F. Southern Ocean seasonal restratification delayed by submesoscale wind–front interactions. *J. Phys. Oceanogr.* **49**, 1035–1053 (2019).

41. Little, H. J., Vichi, M., Thomalla, S. J. & Swart, S. Spatial and temporal scales of chlorophyll variability using high-resolution glider data. *J. Mar. Syst.* **187**, 1–12 (2018).

42. Prend, C. J. et al. Sub-seasonal forcing drives year-to-year variations of Southern Ocean primary productivity. *Global Biogeochem. Cy.* **36**, e2022GB007329 (2022).

43. Swart, S. et al. The Southern Ocean mixed layer and its boundary fluxes: fine-scale observational progress and future research priorities. *Phil. Trans. R. Soc. A* **381**, 20220058 (2023).

44. Thomalla, S. J. et al. Southern Ocean phytoplankton dynamics and carbon export: insights from a seasonal cycle approach. *Phil. Trans. R. Soc. A* **381**, 20220068 (2023).

45. Barton, A. D., Dutkiewicz, S., Flierl, G., Bragg, J. & Follows, M. J. Patterns of diversity in marine phytoplankton. *Science* **327**, 1509–1511 (2010).

46. Finkel, Z. V. et al. Phytoplankton in a changing world: cell size and elemental stoichiometry. *J. Plankton Res.* **32**, 119–137 (2010).

47. Rogers, A. D. et al. Antarctic futures: an assessment of climate-driven changes in ecosystem structure, function, and service provisioning in the Southern Ocean. *Ann. Rev. Mar. Sci.* **12**, 87–120 (2020).

48. Payne, A. J., Vieli, A., Shepherd, A. P., Wingham, D. J. & Rignot, E. Recent dramatic thinning of largest West Antarctic ice stream triggered by oceans. *Geophys. Res. Lett.* **31**, L23401 (2004).

49. Martínez-Moreno, J. et al. Global changes in oceanic mesoscale currents over the satellite altimetry record. *Nat. Clim. Change* **11**, 397–403 (2021).

50. Swart, N. C., Fyfe, J. C., Saenko, O. A. & Eby, M. Wind-driven changes in the ocean carbon sink. *Biogeosciences* **11**, 6107–6117 (2014).

51. Hutchins, D. A. & Boyd, P. W. Marine phytoplankton and the changing ocean iron cycle. *Nat. Clim. Change* **6**, 1072–1079 (2016).

52. Fauchereau, N., Tagliabue, A., Bopp, L. & Monteiro, P. M. S. The response of phytoplankton biomass to transient mixing events in the Southern Ocean. *Geophys. Res. Lett.* **38**, L17601 (2011).

53. Eayrs, C., Li, X., Raphael, M. N. & Holland, D. M. Rapid decline in Antarctic sea ice in recent years hints at future change. *Nat. Geosci.* **14**, 460–464 (2021).

54. Stammerjohn, S. E., Martinson, D. G., Smith, R. C., Yuan, X. & Rind, D. Trends in Antarctic annual sea ice retreat and advance and their relation to El Niño–Southern Oscillation and Southern Annular Mode variability. *J. Geophys. Res. Oceans* **113**, C03S90 (2008).

55. Setzer, A. W., Kayano, M. T., Oliveira, M. R., Ceron, W. L. & Rosa, M. B. Increase in the number of explosive low–level cyclones around King George Island in the last three decades. *An. Acad. Bras. Cienc.* **94**, e20210633 (2022).

56. Gille, S. T. Meridional displacement of the Antarctic Circumpolar Current. *Phil. Trans. R. Soc. A* **372**, 20130273 (2014).

57. Tagliabue, A. et al. Surface-water iron supplies in the Southern Ocean sustained by deep winter mixing. *Nat. Geosci.* **7**, 314–320 (2014).

58. Carranza, M. M. & Gille, S. T. Southern Ocean wind-driven entrainment enhances satellite chlorophyll *a* through the summer. *J. Geophys. Res. Oceans* **120**, 304–323 (2015).

59. Mtshali, T. N. et al. Seasonal depletion of the dissolved iron reservoirs in the sub-Antarctic zone of the southern Atlantic Ocean. *Geophys. Res. Lett.* **46**, 4386–4395 (2019).

60. Fossi, M. C. et al. The role of large marine vertebrates in the assessment of the quality of pelagic marine ecosystems. *Mar. Environ. Res.* **77**, 156–158 (2012).

61. Hückstädt, L. A., McCarthy, M. D., Koch, P. L. & Costa, D. P. What difference does a century make? Shifts in the ecosystem structure of the Ross Sea, Antarctica, as evidenced from a sentinel species, the Weddell seal. *Proc. R. Soc. B* **284**, 20170927 (2017).

62. Hjort, J. *Fluctuations in the Great Fisheries of Northern Europe Viewed in the Light of Biological Research* (Andr. Fred. Host & Fils, 1914).

63. Cushing, D. H. *Marine Ecology and Fisheries* (Cambridge Univ. Press, 1975).

64. Platt, T., Fuentes-Yaco, C. & Frank, K. T. Spring algal bloom and larval fish survival. *Nature* **423**, 398–399 (2003).

65. Barbraud, C. & Weimerskirch, H. Antarctic birds breed later in response to climate change. *Proc. Natl Acad. Sci. USA* **103**, 6248–6251 (2006).

66. Dawbin, W. H. in *Whales, Dolphins, and Porpoises* (ed. Norris, K. S.) Ch. 9 (Univ. California Press, 1966).

67. Ramp, C., Delarue, J., Palsbøll, P. J., Sears, R. & Hammond, P. S. Adapting to a warmer ocean—seasonal shift of baleen whale movements over three decades. *PLoS ONE* **10**, e0121374 (2015).

68. Avila, I. C., Dormann, C. F., García, C., Payán, L. F. & Zorrilla, M. X. Humpback whales extend their stay in a breeding ground in the tropical eastern Pacific. *ICES J. Mar. Sci.* **77**, 109–118 (2020).

69. Seyboth, E. et al. Southern right whale (*Eubalaena australis*) reproductive success is influenced by krill (*Euphausia superba*) density and climate. *Sci. Rep.* **6**, 28205 (2016).

70. Croxall, J. P., Trathan, P. N. & Murphy, E. J. Environmental change and Antarctic seabird populations. *Science* **297**, 1510–1514 (2002).

Methods

Satellite-derived chl-*a* concentrations were obtained from the European Space Agency Ocean Colour Climate Change Initiative (https://esa-oceancolour-cci.org ref. 71) at 4 km and 8 day resolution (v.6.0). Analyses covered the period from 4 September 1997 to 27 December 2022 for the Southern Ocean biomes as defined in ref. 28, the STSS, the SPSS and the ICE. To reduce missing data, chl-*a* values were first regridded to a regular 25 km grid through bilinear interpolation using the xESMF Python package[72]. The remaining gaps were filled by applying a linear interpolation scheme in sequential steps of longitude, latitude and time[73] using a three-point window. If one of the points bordering the gap along the indicated axis was invalid, it was omitted from the calculation; if two surrounding points were invalid, then the gap was not filled. Finally, the data were smoothed by applying a moving average filter of the previous and next time steps. For more details on this method, see ref. 74.

Seasonal metrics

Phytoplankton blooms typically manifest as a seasonal cycle, with a bloom initiation that identifies the timing of the ramp-up in phytoplankton growth and biomass accumulation followed by bloom peaks within the growing season (which could be multiple) and finally the bloom termination, which defines the end of the growing season[27,75–79]. The calculation of the phenological indices of bloom initiation, termination and duration followed closely the methods of ref. 26, detailed in the following, but with some additional steps (see Supplementary Fig. 1 for examples of the phenological indices described).

(1) Bloom slice: each pixel and year's 'bloom slice' was found by locating the timing of the climatological mean bloom maximum then centring the bloom slice per year that starts and ends at the preceding and following 6 months, respectively.

(2) Bloom maximum chl-*a*: the bloom maximum was identified as the local maximum in chl-*a* that occurs within this bloom slice.

(3) Bloom initiation: the bloom initiation date for each bloom slice was calculated by first determining the minimum before the bloom maximum and the range, as the difference in chl-*a* concentration between the bloom maximum and the preceding minimum. The bloom initiation was then determined as the first date after the pre-peak minimum that the chl-*a* concentration was greater than the minimum chl-*a* concentration plus 5% of the chl-*a* range.

(4) Bloom termination: the bloom termination date for each bloom slice was similarly calculated as the first date after the bloom maximum that the chl-*a* concentration was less than the chl-*a* concentration at the minimum plus 5% of the range. However, to ensure that seasonal blooms with more than one peak could be accounted for, multiple bloom peaks were defined as a second, third or *n*th local maxima where the chl-*a* concentration reached at least 75% of the amplitude of the bloom maximum defined in (2) and was a minimum of 24 days (3 ×8 day time intervals) from the maximum peak. The additional peaks were identified with the Python SciPy[80] function 'find_peaks'. In these instances, the six-month time span for either initiation or termination was calculated from the first or last peak, respectively.

(5) Bloom duration: the bloom duration was calculated as the number of days between the bloom initiation and termination dates.

(6) Bloom mean chl-*a*: the mean chl-*a* over bloom duration was calculated as the mean chl-*a* concentration between the bloom initiation and termination dates.

(7) Bloom integrated chl-*a*: the seasonally integrated bloom chl-*a* was calculated using the NumPy[81] trapezoidal function as the chl-*a* concentration integrated between the bloom initiation and termination dates.

Additional methods for calculating bloom initiation, bloom termination, bloom duration, bloom mean chl-*a* and bloom integrated chl-*a* were used to test the sensitivity of the choice in phenological methods.

These included the cumulative-sum method and the rate-of-change method[33], where the cumulative-sum method is defined as the first moment the cumulative chl-*a* biomass surpasses 15% of the total biomass, and the rate-of-change method is derived as the first moment the first derivative surpasses 15% of the median derivative. Results from the other methods are presented in Extended Data Figs. 4–6 for comparison.

(8) SCR: the reproducibility of the annual seasonal cycle was calculated by first generating a climatological mean seasonal cycle by resampling the time series to a monthly climatological mean that was then averaged across all years to generate a climatology and subsequently interpolated to 46 data points (the same number of 8-day timesteps per year as in the original chl-*a* dataset). The SCR is then calculated as the Pearson's correlation coefficient of the annual seasonal cycle against the climatological mean seasonal cycle. A value of 100% is indicative of an annual seasonal cycle that is a perfect replica of the climatological mean, while a value of 0% implies no relationship between the annual seasonal cycle and the climatological mean. Unlike for seasonal metrics (1)–(7), for SCR no 3× time step (3 × 8 day) rolling mean was applied to the regridded and interpolated data. All phenological indices data are publicly available[82].

Two adjusted methods of calculating SCR were performed to test robustness and susceptibility to possible bias. (1) The time series was detrended before calculating the 25-year climatology and then correlated with each year to determine the percentage SCR. (2) Each year was correlated against a rolling five-year climatology (instead of a 25-year climatology) centred on the year in question to determine percentage SCR. Note that this approach requires the first and second years of the time series to be correlated against a climatology that is generated from only three and four years, respectively (as do the last and second-to-last years of the time series). Results from these approaches are presented in Extended Data Figs. 7 and 8 for comparison.

The cyclical nature of the calendar poses a considerable issue that needs to be addressed when calculating means of phenological indices. For example, we need to avoid a situation where the mean bloom initiation between a year with a bloom in December (for example, day of year = 340) and a year with a bloom in January (for example, day of year = 10) is incorrectly calculated as an average bloom initiation date in June (for example, day of year = 175). To account for this, we used the Python SciPy[80] function 'circmean', which calculates circular means for samples in a range (correct mean = day of year 357).

Trend calculations

The cyclical nature of the calendar similarly poses a problem when examining trends in dates for bloom initiation, termination and the timing of the bloom maximum. To account for this, trends in dates were calculated from the difference in days between each time step and the mean date, that is, the anomaly from the climatological mean phenological date.

Any pixel whose time series had less than 50% of the data available was excluded from any statistical trend analysis. Before linear regressions were performed on the trends, the data were first tested for a normal distribution. If the data were normally distributed, then linear regressions were performed using the Sci-Kit[83] Huber Regressor ($\varepsilon = 1.35$). If the data were not normally distributed, then linear regressions were performed using the non-parametric Mann–Kendall test[84]. All linear regression statistics are reported at the 95% probability, $P < 0.05$. A sensitivity test of varying ε between 1.2 and 1.5 altered the proportion of trends significant across the Southern Ocean but never by more than 12% (Supplementary Fig. 2).

To examine potential regime shifts across the Southern Ocean, mean chl-*a* concentrations were calculated using log transformation. The limits for different regimes were a mean chl-*a* of 0.25 mg m^{-3} and a mean SCR r^2 of 40%. The four regimes were defined as follows: low chl-*a* + low SCR, low chl-*a* + high SCR, high chl-*a* + low SCR and high chl-*a* + high SCR.

Driver analysis

To investigate the possible response of phytoplankton phenology to annual changes in the occurrence of high-speed wind events, we include a windiness metric that counts the occurrence of high wind speeds, defined as the number of days per year in which the daily averaged wind speeds are greater than the 25-year 75th percentile of all wind speeds (the percentile is calculated over 1998–2022). This was computed using reanalysis wind speeds between 1998 and 2022 from the Japanese 55-year Reanalysis[85]. For SST, we used the Group for High Resolution Sea Surface Temperature (https://www.ghrsst.org/). MLD data were computed from Hadley EN4.2.2 gridded temperature and salinity profiles[86] after conversion to potential density using a gradient of 0.03 kg m^{-3}(ref. 87). SST, MLD and wind data were spatially correlated with phenological indices using Pearson correlation coefficients.

Reporting summary

Further information on research design is available in the Nature Portfolio Reporting Summary linked to this article.

Data availability

All data used in this study are available publicly[82]. Surface chlorophyll *a* is available from the Ocean Colour–CCI dataset (v.6.0) at https://esa-oceancolour-cci.org. Wind data used in this study are from the Japanese 55-year Reanalysis (JRA-55-do); data are available at https://esgf-node.llnl.gov/search/input4mips/. To search, select "Target MIP" = "OMIP", "Institution ID" = "MRI" and "Source Version" = "1.4.0" among tabs on the left side. The sea surface temperature data used in this study are available at https://www.ghrsst.org. The gridded temperature and salinity profiles used to derive the mixed-layer depth are available at https://www.metoffice.gov.uk/hadobs/en4/download-en4-2-2.html. All phenology output data are available at https://doi.org/10.5281/zenodo.8087125 ref. 82.

Code availability

Data analyses were conducted in Python 3.7. All python packages used for the calculations are publicly available and referenced.

References

71. Sathyendranath, S. et al. An ocean-colour time series for use in climate studies: the experience of the Ocean-Colour Climate Change Initiative (OC-CCI). *Sensors* **19**, 4285 (2019).
72. Zhuang, J. et al. pangeo-data/xESMF: v0.7.1. *Zenodo* https://doi.org/10.5281/ZENODO.7800141 (2023).
73. Racault, M.-F., Sathyendranath, S. & Platt, T. Impact of missing data on the estimation of ecological indicators from satellite ocean-colour time-series. *Remote Sens. Environ.* **152**, 15–28 (2014).
74. Salgado-Hernanz, P. M., Racault, M.-F., Font-Muñoz, J. S. & Basterretxea, G. Trends in phytoplankton phenology in the Mediterranean Sea based on ocean-colour remote sensing. *Remote Sens. Environ.* **221**, 50–64 (2019).
75. Henson, S. A., Dunne, J. P. & Sarmiento, J. L. Decadal variability in North Atlantic phytoplankton blooms. *J. Geophys. Res. Oceans* **114**, C04013 (2009).
76. Siegel, D. A., Doney, S. C. & Yoder, J. A. The North Atlantic spring phytoplankton bloom and Sverdrup's critical depth hypothesis. *Science* **296**, 730–733 (2002).
77. Racault, M. F., Le Quéré, C., Buitenhuis, E., Sathyendranath, S. & Platt, T. Phytoplankton phenology in the global ocean. *Ecol. Indic.* **14**, 152–163 (2012).
78. Vargas, M., Brown, C. W. & Sapiano, M. R. P. Phenology of marine phytoplankton from satellite ocean color measurements. *Geophys. Res. Lett.* **36**, L01608 (2009).
79. Greve, W., Prinage, S., Zidowitz, H., Nast, J. & Reiners, F. On the phenology of North Sea ichthyoplankton. *ICES J. Mar. Sci.* **62**, 1216–1223 (2005).
80. Virtanen, P. et al. SciPy 1.0: fundamental algorithms for scientific computing in Python. *Nat. Methods* **17**, 261–272 (2020).
81. Harris, C. R. et al. Array programming with NumPy. *Nature* **585**, 357–362 (2020).
82. Thomalla, S., Nicholson, S., Ryan-Keogh, T. & Smith, M. Widespread changes in Southern Ocean phytoplankton blooms linked to climate drivers. *Zenodo* https://doi.org/10.5281/ZENODO.8087125 (2023).
83. Pedregosa, F. et al. Scikit-learn: machine learning in Python. *J. Mach. Learn. Res.* **85**, 2825–2830 (2011).
84. Hussain, M. M. & Mahumd, I. pyMannKendall: a python package for non parametric Mann Kendall family of trends tests. *J. Open Source Softw.* **4**, 1556 (2019).
85. Tsujino, H. et al. JRA-55 based surface dataset for driving ocean–sea-ice models (JRA55-do). *Ocean Model* **130**, 79–139 (2018).
86. Good, S. A., Martin, M. J. & Rayner, N. A. EN4: quality controlled ocean temperature and salinity profiles and monthly objective analyses with uncertainty estimates. *J. Geophys. Res. Oceans* **118**, 6704–6716 (2013).
87. de Boyer Montégut, C., Madec, G., Fischer, A. S., Lazar, A. & Iudicone, D. Mixed layer depth over the global ocean: an examination of profile data and a profile-based climatology. *J. Geophys. Res. Oceans* **109**, C12003 (2004).

Acknowledgements

Author contributions

S.J.T. conceptualized this study with all authors contributing to the methodology and interpretation of results. Formal analysis was done by S.-A.N., T.J.R.-K. and M.E.S. Software was developed by S.-A.N. and T.J.R.-K., with T.J.R.-K. producing all visualizations. The original draft was written by S.J.T. with all authors contributing to the review and editing of the original draft.

Competing interests

The authors declare no competing interests.

Additional information

Extended data is available for this paper at https://doi.org/10.1038/s41558-023-01768-4.

Supplementary information The online version contains supplementary material available at https://doi.org/10.1038/s41558-023-01768-4.

Correspondence and requests for materials should be addressed to Sandy J. Thomalla.

Peer review information *Nature Climate Change* thanks Tyler Rohr, Shubha Sathyendranath and the other, anonymous, reviewer(s) for their contribution to the peer review of this work.

Reprints and permissions information is available at www.nature.com/reprints.
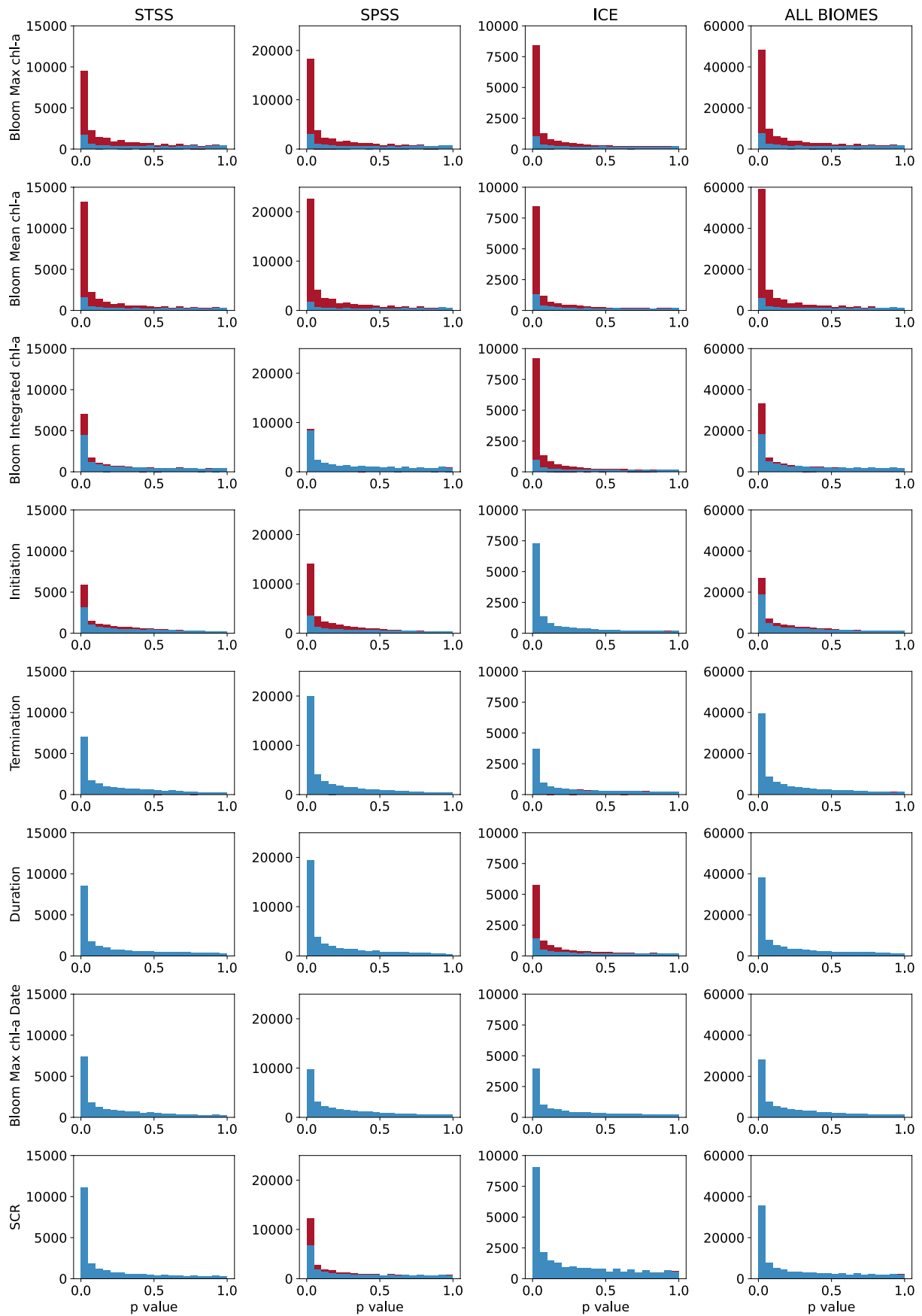
**Extended Data Fig. 1 | See next page for caption.**

Extended Data Fig. 1 | Histogram plots depicting the distribution of p values for the trends in phytoplankton seasonal metrics. All p values are plotted for all pixels and distinguished between either negative (blue) or positive (red) trends for each seasonal metric in each biome and for the Southern Ocean as a whole. The seasonal metrics are from top to bottom: bloom max chlorophyll (Max chl-a), mean chl-a over bloom duration (Bloom Mean chl-a), integrated chl-a over bloom duration (Bloom Integrated chl-a), bloom initiation, bloom termination, bloom duration, Bloom Max chla-a date and seasonal cycle reproducibility (SCR). The Fay and McKinley[28] biomes are from left to right: the subtropical seasonally stratified (STSS), the subpolar seasonally stratified (SPSS), the ice (ICE) biome and all three biomes merged (ALL). Phenological indices are determined using the threshold method of detection.
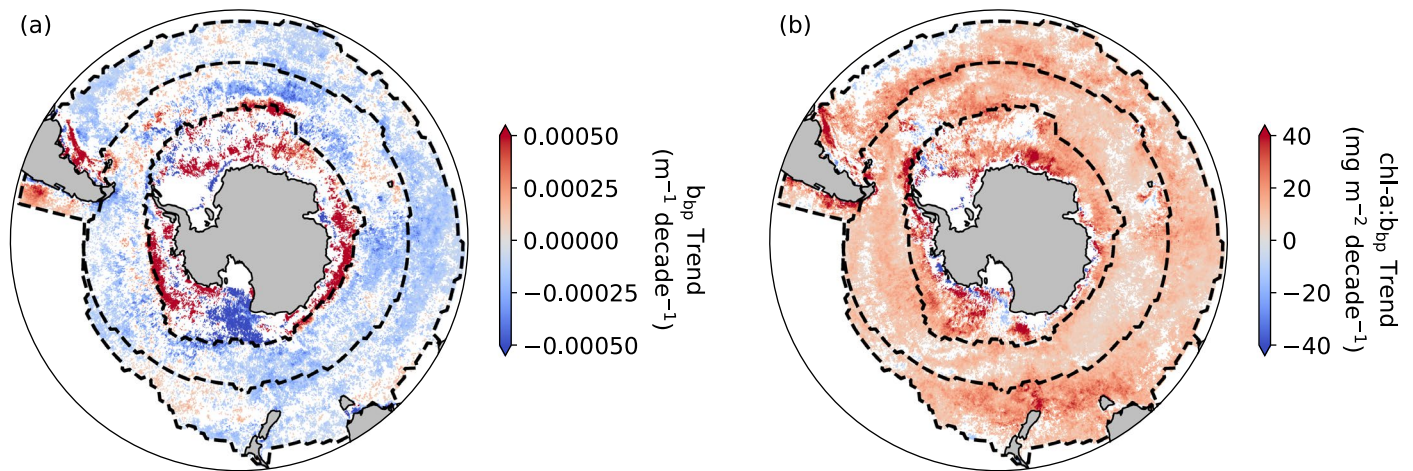
Extended Data Fig. 2 | Regional distribution of trends in backscatter and the ratio between chlorophyll and backscatter. Decadal trends [1998 – 2022] of a) backscatter (b_{bp}) as proxy for phytoplankton carbon and an independent determinant of phytoplankton biomass and b) the chlorophyll (chl-a) to b_{bp} ratio (chl-a:bbp). b_{bp} data at a wavelength of 443 nm (λ443) was downloaded from the OC-CCI server (v6.0) and processed in the same way as chl-a. Only pixels where trends were significant (p < 0.05) and where >50% of the time series per year was available have been plotted, non-significant trends (p > 0.05) and incomplete time series are presented as white.
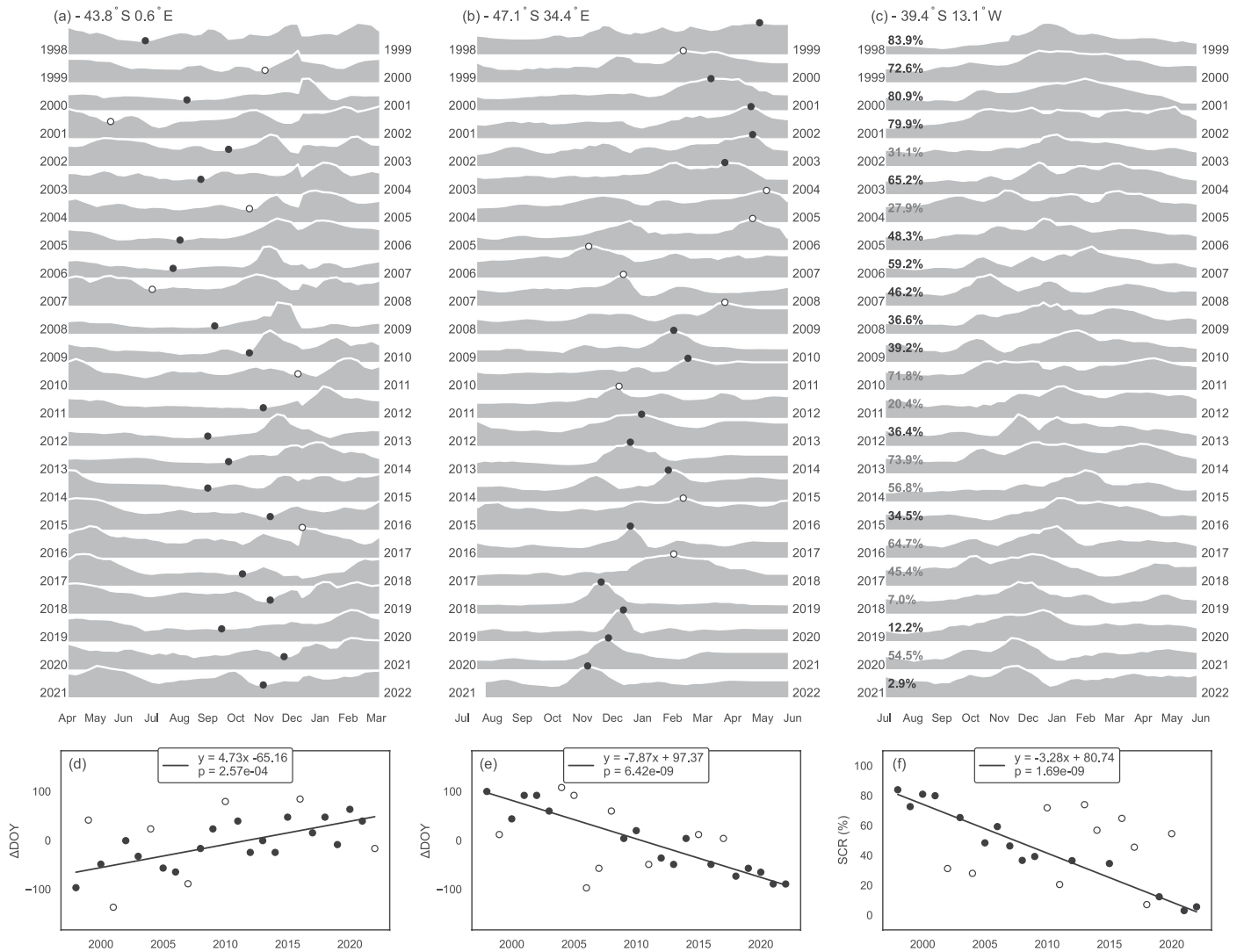
Extended Data Fig. 3 | Visual representation of trends in phytoplankton seasonal metrics from three example pixels. Ridgeline plots highlight (a) the change in bloom initiation at (43.8°S, 0.6°E) of 47.26 days decade-1 (b) the change in bloom maximum date at (47.1°S, 34.4°E) of -78.96 days decade-1 and (c) the change in SCR at (39.4°S, 13.1°W) of -29.40% decade-1. Linear regressions of (d) the bloom initiation from panel a, (e) the bloom maximum date from panel b and (f) the SCR from panel c. Please note the different x-axis in panel a. In panels a, b, d, e and f, outliers as identified by the Huber-Loss regression are differentiated as white circles, and in panel c the outliers in SCR % are depicted in grey. The statistics of all seasonal metrics for each example pixel can be found in Table ED3.
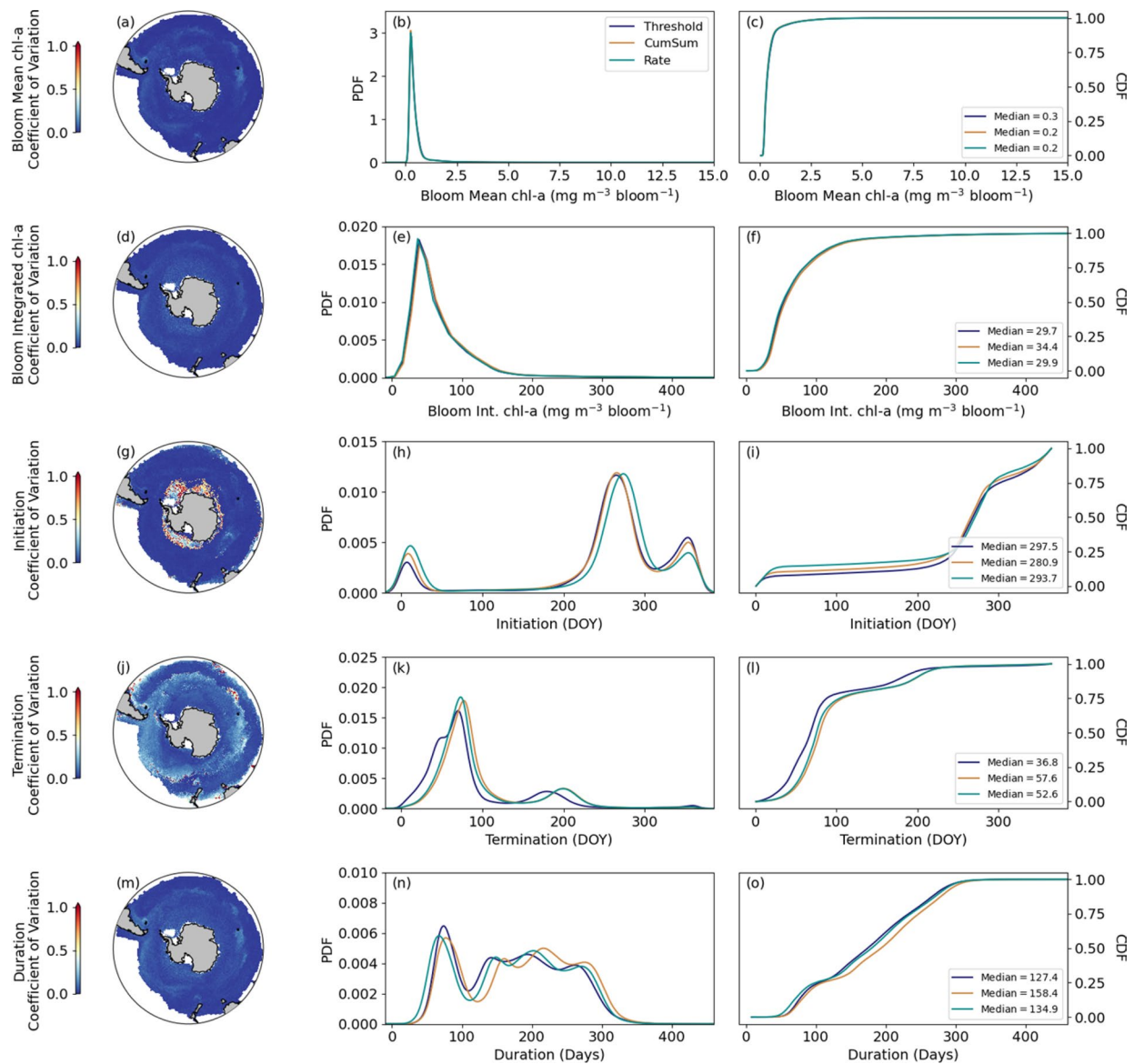
Extended Data Fig. 4 | Comparing the distribution of phytoplankton seasonal metrics using three different methods of detection. Here three methods of detecting bloom phenology are compared: the Threshold method (this study) in dark blue, the cumulative sum method[35] (CumSum) in orange and the rate of change method[35] (Rate) in turquoise. Maps on the left depict the regional distribution of the coefficient of variation (calculated as the inter-method standard deviation normalised to the inter-method mean), in the middle is the probability distributions (PDF) of the climatological mean [1998-2022] from each of the three methods and on the right is the cumulative distributions (CDF) for the three methods for the climatological mean [1998-2022] maps of phenological metrics of bloom mean chlorophyll (chl-a) (a, b, c), bloom integrated chl-a (d,e,f), bloom initiation (g,h,i), bloom termination (j,k,l) and bloom duration (m,n,o).
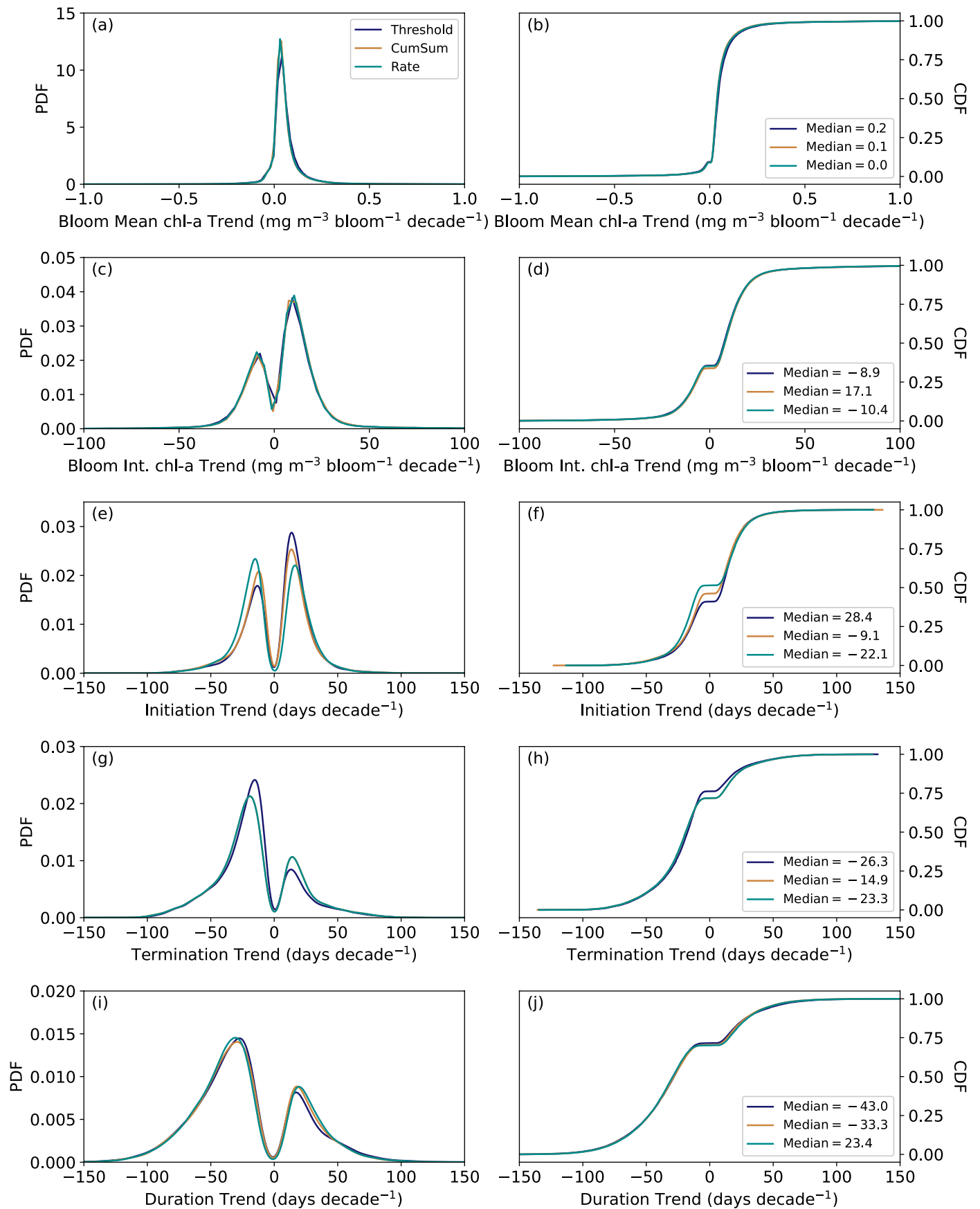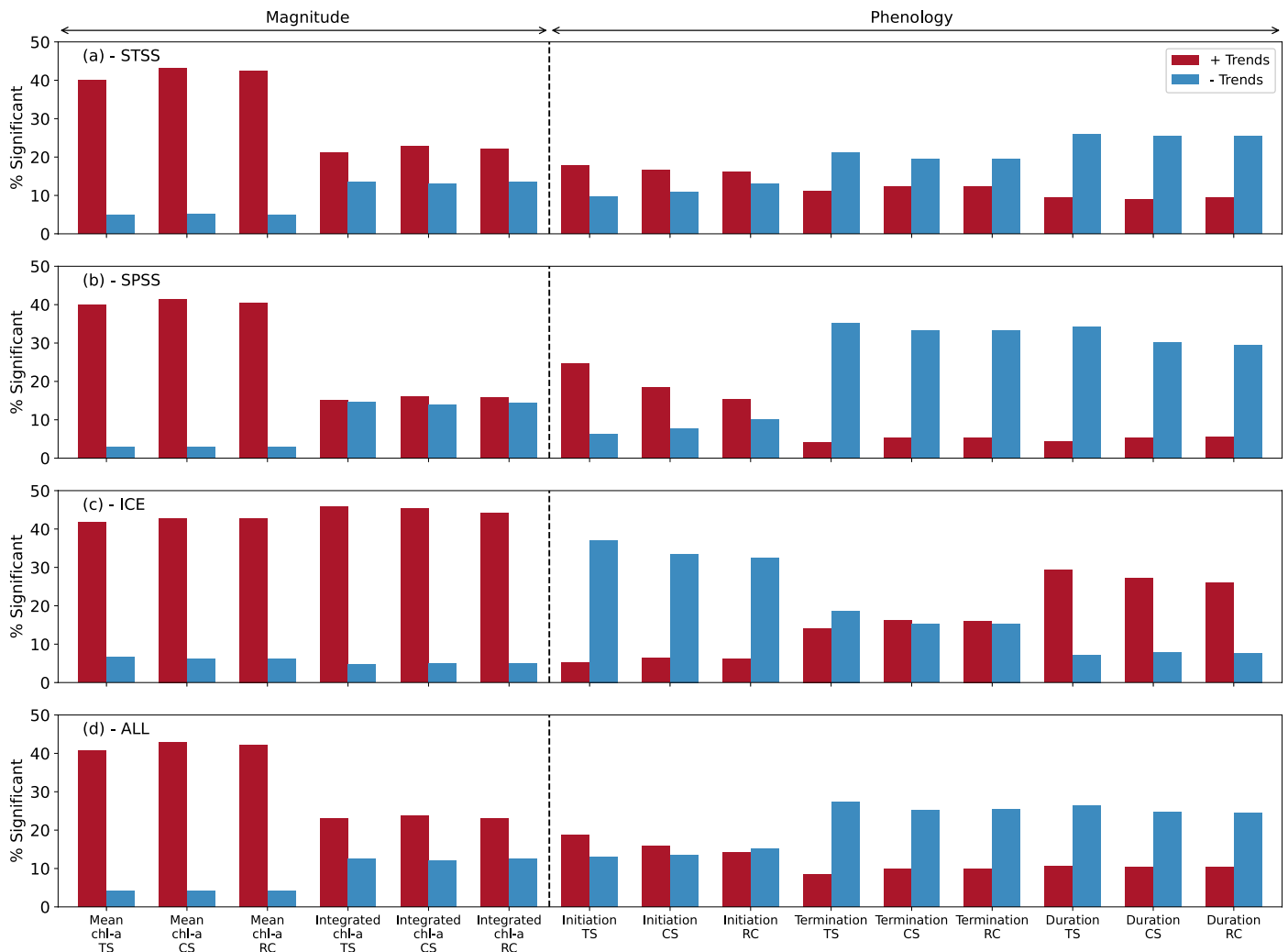
Extended Data Fig. 5 | See next page for caption.

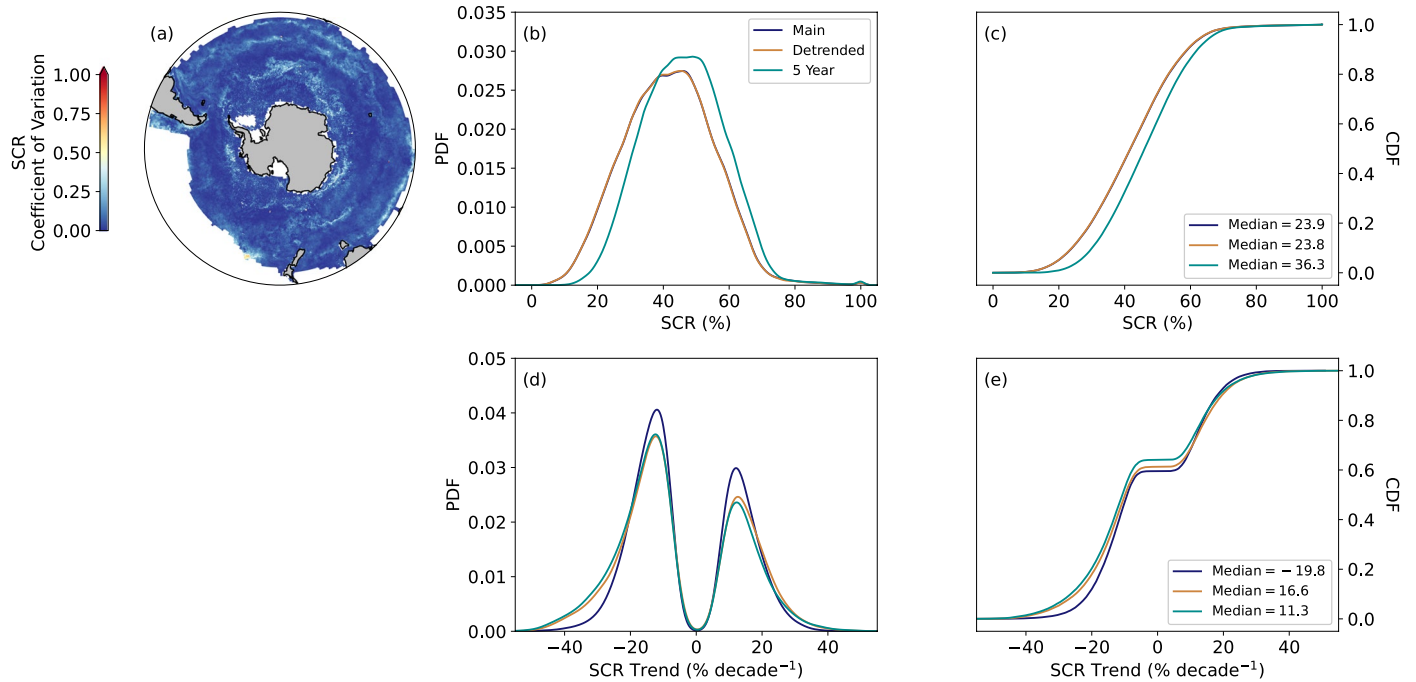**Extended Data Fig. 5 | Comparing the distribution of trends in phytoplankton seasonal metrics from three different methods of detection.** Here the significant ($p < 0.05$) decadal trends [1998 – 2022] in seasonal metrics are compared using three methods of detecting bloom phenology: the threshold method (this study) in dark blue, the cumulative sum method[35] (CumSum) in orange and the rate of change method[35] (Rate) in turquoise. On the left is the probability distributions (PDF) of the significant trends from each of the three methods and to the right is the cumulative distributions (CDF) from the three methods of the significant trends in bloom mean chl-a (a, b), bloom integrated chl-a (c, d), bloom initiation (e, f), bloom termination (g, h) and bloom duration (i, j).
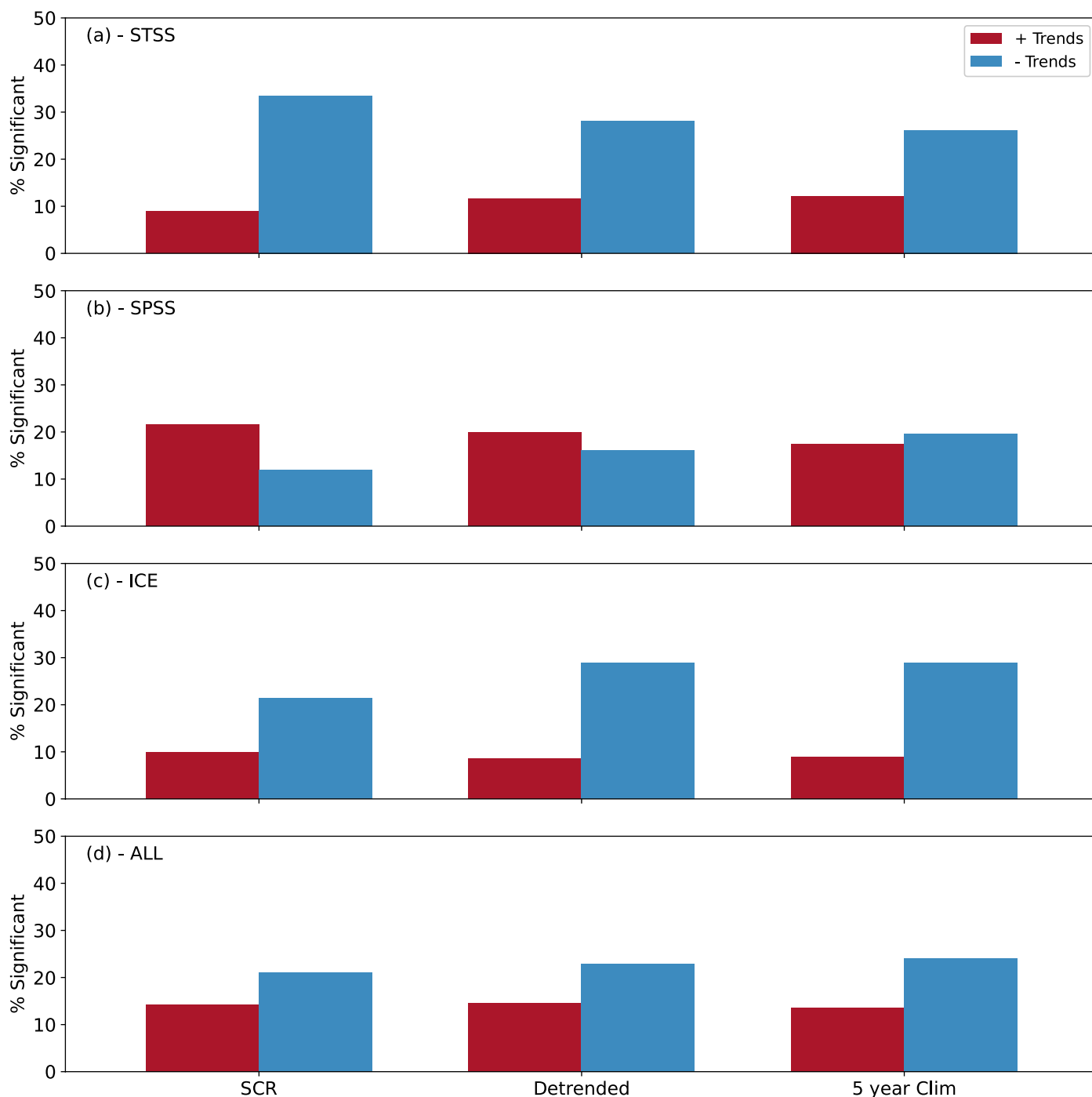
Extended Data Fig. 6 | Bar graph depicting regional dominance in the direction of significant trends in phytoplankton seasonal metrics from three different methods of detection. Bars depict the % of pixels with significant (p < 0.05) positive (red) or negative (blue) trends per seasonal cycle metric relative to the total number of pixels per biome and for the Southern Ocean as a whole. The three methods of detection are the threshold method from this study (TS), the cumulative sum (CS) method[35] and the rate of change (RC) method[35]. The seasonal metrics are from left to right: mean chl-a over bloom duration (Mean chl-a), integrated chl-a over bloom duration (Integrated chl-a), bloom initiation, bloom termination and bloom duration. The Fay and McKinley[28] biomes are from top to bottom: the subtropical seasonally stratified (STSS), the subpolar seasonally stratified (SPSS), the ice (ICE) biome and all three biomes merged (ALL).

Extended Data Fig. 7 | Comparing the distribution of seasonal cycle reproducibility (SCR) calculated in three different ways. Here we compare SCR calculated as 1) Main: the correlation between the observed annual chl-a time series and the mean climatological seasonal cycle (that is, the main method used in this study in dark blue), 2) Detrended: the correlation between the observed annual chl-a time series and a detrended climatology (in orange) and 3) 5 year: the correlation between the observed annual chl-a time series and a 5-year rolling mean climatology centred on the year in question (in turquoise).

The map a) depicts the distribution of the coefficient of variation (calculated as the inter-approach standard deviation normalised to the inter-approach mean) b) is the probability distributions (PDF) of the climatological mean [1998-2022] SCR from each of the three approaches c) is the cumulative distributions (CDF) for the climatological mean [1998-2022] SCR for the three approaches, d) is the PDF of the significant trends ($p < 0.05$) in SCR for the three approaches and e) is the CDF for the significant trends ($p < 0.05$) in SCR for the three approaches.

Extended Data Fig. 8 | Bar graph depicting regional dominance in the direction of significant trends in Seasonal Cycle Reproducibility (SCR) using three different methods of detection. Bars depict the % of pixels with significant (p < 0.05) positive (red) or negative (blue) trends in SCR relative to the total number of pixels per biome and for the Southern Ocean as a whole. The three methods from left to right are calculated as the correlation of the observed annual chl-a time series against the mean climatological seasonal cycle (that is, the main method of SCR used in this study), a detrended climatology (Detrended) and a 5-year rolling mean climatology centred on the year in question (5 year Clim). The Fay and McKinley[28] biomes are from top to bottom: the subtropical seasonally stratified (STSS), the subpolar seasonally stratified (SPSS), the ice (ICE) biome and all three biomes merged (ALL).
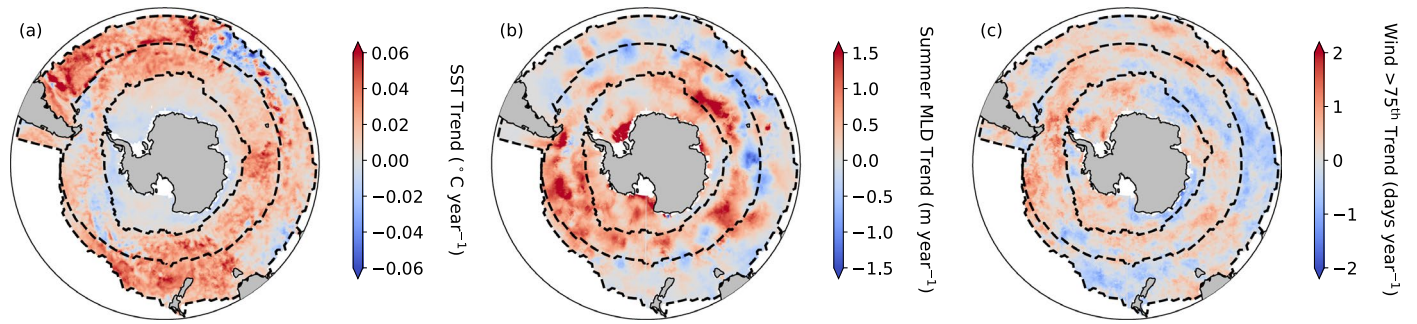
Extended Data Fig. 9 | Regional distribution of trends in physical drivers. Decadal trends [1998 – 2022] of (a) sea surface temperature (SST; °C m^{-1} day^{-1}), (b) summer mixed layer depth (MLD; m year^{-1}) and (c) windiness (that is, number of days per year where the wind speed is greater than the 25 year 75th percentile (trend analysis performed as per phenological indices). Note that both significant (p < 0.05) and non-significant (p > 0.05) trends are plotted.
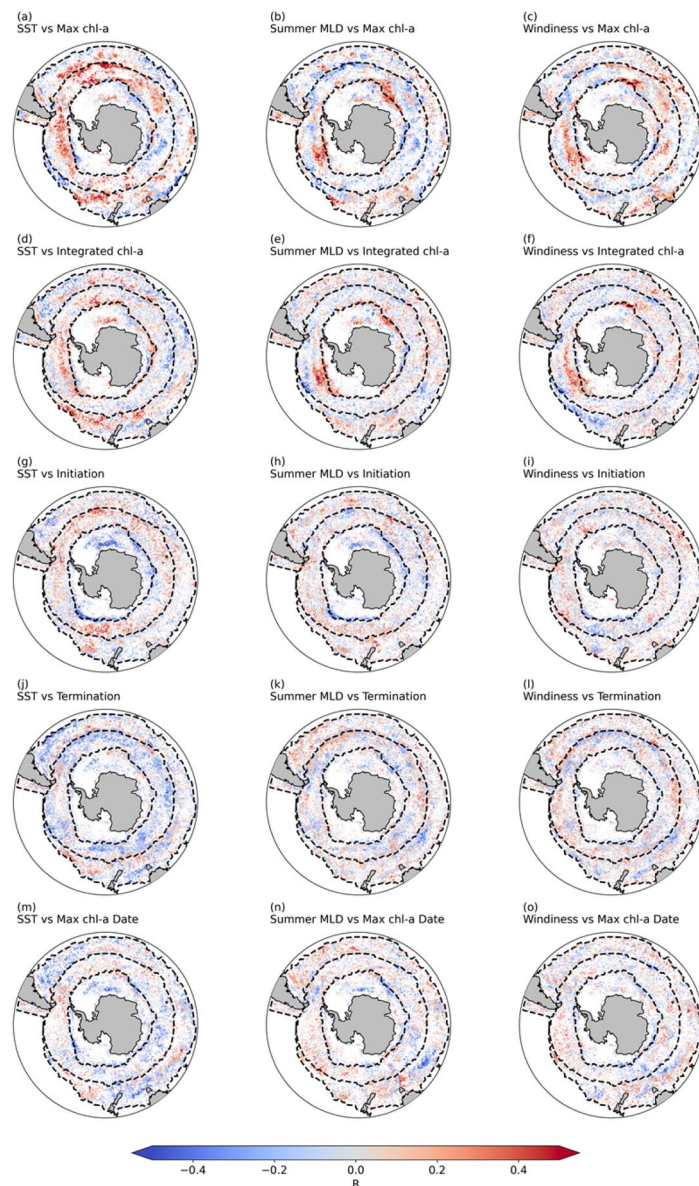
Extended Data Fig. 10 | Regional distribution of the correlation between physical drivers and the remaining phytoplankton seasonal metrics (selected subset in Fig. 4). Maps depict the spatial correlation of (a,b,c) maximum bloom chlorophyll-a (chl-a), (d,e,f) integrated bloom chl-a, (g,h,i) bloom initiation, (j,k,l) bloom termination, and (m,n,o) maximum chl-a date against sea surface temperature (SST) on the left, summer mixed layer depth (MLD) in the middle and windiness (that is number of days per year that wind was greater than the 25 year 75th percentile) on the right. Data were excluded if less than 50% of either time series per year was available. Correlations are performed against the corresponding 25 years of SST, MLD and windiness data (1998 - 2022), with data only plotted if the seasonal cycle metric trend is significant.

nature portfolio

Corresponding author(s): Sandy J. Thomalla, Sarah-Anne Nicholson, Thomas J. Ryan-Keogh, Marié E. Smith

Last updated by author(s): 30 June 2023

Reporting Summary

Nature Portfolio wishes to improve the reproducibility of the work that we publish. This form provides structure for consistency and transparency in reporting. For further information on Nature Portfolio policies, see our Editorial Policies and the Editorial Policy Checklist.

Statistics

For all statistical analyses, confirm that the following items are present in the figure legend, table legend, main text, or Methods section.

n/a	Confirmed	
☒	☐	The exact sample size (*n*) for each experimental group/condition, given as a discrete number and unit of measurement
☒	☐	A statement on whether measurements were taken from distinct samples or whether the same sample was measured repeatedly
☐	☒	The statistical test(s) used AND whether they are one- or two-sided *Only common tests should be described solely by name; describe more complex techniques in the Methods section.*
☒	☐	A description of all covariates tested
☐	☒	A description of any assumptions or corrections, such as tests of normality and adjustment for multiple comparisons
☐	☒	A full description of the statistical parameters including central tendency (e.g. means) or other basic estimates (e.g. regression coefficient) AND variation (e.g. standard deviation) or associated estimates of uncertainty (e.g. confidence intervals)
☒	☐	For null hypothesis testing, the test statistic (e.g. *F*, *t*, *r*) with confidence intervals, effect sizes, degrees of freedom and *P* value noted *Give P values as exact values whenever suitable.*
☒	☐	For Bayesian analysis, information on the choice of priors and Markov chain Monte Carlo settings
☒	☐	For hierarchical and complex designs, identification of the appropriate level for tests and full reporting of outcomes
☒	☐	Estimates of effect sizes (e.g. Cohen's *d*, Pearson's *r*), indicating how they were calculated

Our web collection on statistics for biologists contains articles on many of the points above.

Software and code

Policy information about availability of computer code

Data collection	All data used in this study are available publicly. Surface chlorophyll-a are available from the Ocean Colour-CCI dataset (v6.0) at https://esa-oceancolour-cci.org. Wind data used in this study is from the Japanese 55-year Reanalysis (JRA-55-do) data are available at https://esgf-node.llnl.gov/search/input4mips/. To search, select "Target MIP"="OMIP", "Institution ID"="MRI", and "Source Version"="1.4.0" among tabs on the left side. The sea surface temperature data used in this study are available at https://www.ghrsst.org. The gridded temperature and salinity profiles used to derive the mixed layer depth are available at https://www.metoffice.gov.uk/hadobs/en4/download-en4-2-2.html.
Data analysis	Data analyses were conducted in Python 3.7. All python packages used for the calculations are publicly available and referenced.

For manuscripts utilizing custom algorithms or software that are central to the research but not yet described in published literature, software must be made available to editors and reviewers. We strongly encourage code deposition in a community repository (e.g. GitHub). See the Nature Portfolio guidelines for submitting code & software for further information.

Data

All manuscripts must include a data availability statement. This statement should provide the following information, where applicable:

- Accession codes, unique identifiers, or web links for publicly available datasets
- A description of any restrictions on data availability
- For clinical datasets or third party data, please ensure that the statement adheres to our policy

All phenology output data are available at: https://doi.org/10.5281/zenodo.8087125.

Research involving human participants, their data, or biological material

Reporting on sex and gender	*Use the terms sex (biological attribute) and gender (shaped by social and cultural circumstances) carefully in order to avoid confusing both terms. Indicate if findings apply to only one sex or gender; describe whether sex and gender were considered in study design; whether sex and/or gender was determined based on self-reporting or assigned and methods used. Provide in the source data disaggregated sex and gender data, where this information has been collected, and if consent has been obtained for sharing of individual-level data; provide overall numbers in this Reporting Summary. Please state if this information has not been collected. Report sex- and gender-based analyses where performed, justify reasons for lack of sex- and gender-based analysis.*
Reporting on race, ethnicity, or other socially relevant groupings	*Please specify the socially constructed or socially relevant categorization variable(s) used in your manuscript and explain why they were used. Please note that such variables should not be used as proxies for other socially constructed/relevant variables (for example, race or ethnicity should not be used as a proxy for socioeconomic status). Provide clear definitions of the relevant terms used, how they were provided (by the participants/respondents, the researchers, or third parties), and the method(s) used to classify people into the different categories (e.g. self-report, census or administrative data, social media data, etc.) Please provide details about how you controlled for confounding variables in your analyses.*
Population characteristics	*Describe the covariate-relevant population characteristics of the human research participants (e.g. age, genotypic information, past and current diagnosis and treatment categories). If you filled out the behavioural & social sciences study design questions and have nothing to add here, write "See above."*
Recruitment	*Describe how participants were recruited. Outline any potential self-selection bias or other biases that may be present and how these are likely to impact results.*
Ethics oversight	*Identify the organization(s) that approved the study protocol.*

Note that full information on the approval of the study protocol must also be provided in the manuscript.

Field-specific reporting

Please select the one below that is the best fit for your research. If you are not sure, read the appropriate sections before making your selection.

☐ Life sciences ☐ Behavioural & social sciences ☒ Ecological, evolutionary & environmental sciences

For a reference copy of the document with all sections, see nature.com/documents/nr-reporting-summary-flat.pdf

Ecological, evolutionary & environmental sciences study design

All studies must disclose on these points even when the disclosure is negative.

Study description	This study focuses on 25 years of satellite remote sensing chlorophyll data for the Southern Ocean which is used to identify characteristics of the seasonal cycle (regional distribution of the mean state) and how those seasonal metrics change over 25 years (regional distribution of significant trends).
Research sample	Satellite-derived chl-a concentrations were obtained from the European Space Agency ocean colour climate change initiative (OC-CCI; https://esa-oceancolour-cci.org; 69) at 4 km and 8 day resolution (v6.0). Windiness was computed using reanalysis wind speeds between 1998 – 2022 from the Japanese 55-year Reanalysis (JRA-55-do82). For SST we used the Group for High Resolution Sea Surface Temperature (GHRSST; https://www.ghrsst.org/). MLD data were computed from Hadley EN4.2.2 gridded temperature and salinity profiles83 after conversion to potential density using a gradient of 0.03 kg m-3 84.
Sampling strategy	Before linear regressions were performed on the trends, the data were first tested for a normal distribution. If the data were normally distributed, then linear regressions were performed using the Sci-Kit80 Huber-Regressor (ε = 1.35). If the data were not

normally distributed, then linear regressions were performed using the non-parametric Mann-Kendall Test81. All linear regression statistics are reported at the 95% probability, p<0.05.

Data collection	Downloaded from publicly available sites
Timing and spatial scale	Analyses covered the period from 04/09/1997 – 27/12/2022 for the Southern Ocean biomes as defined in Fay & McKinley28
Data exclusions	Any pixel whose time series had less than 50% of the data available were excluded from any statistical trend analysis.
Reproducibility	NA
Randomization	Data were grouped into Southern Ocean biomes; the subtropical seasonally stratified (STSS), the subpolar seasonally stratified (SPSS) and the ice (ICE) biomes as defined by Fay and McKinley28
Blinding	NA

Did the study involve field work? ☐ Yes ☒ No

Reporting for specific materials, systems and methods

We require information from authors about some types of materials, experimental systems and methods used in many studies. Here, indicate whether each material, system or method listed is relevant to your study. If you are not sure if a list item applies to your research, read the appropriate section before selecting a response.

Materials & experimental systems

n/a	Involved in the study
☒	Antibodies
☒	Eukaryotic cell lines
☒	Palaeontology and archaeology
☒	Animals and other organisms
☒	Clinical data
☒	Dual use research of concern
☒	Plants

Methods

n/a	Involved in the study
☒	ChIP-seq
☒	Flow cytometry
☒	MRI-based neuroimaging